Master's thesis

NTNU
Norwegian University of Science and Technology
Faculty of Engineering
Department of Geoscience and Petroleum

Jonas Kristensen Kimerud

Dating of Late Jurassic Black Shales on the Norwegian Shelf by Magnetic Cyclostratigraphy

Master's thesis in Geology
Supervisor: Professor Maarten Felix
June 2020

NTNU
Kunnskap for en bedre verden

Jonas Kristensen Kimerud

Dating of Late Jurassic Black Shales on the Norwegian Shelf by Magnetic Cyclostratigraphy

Master's thesis in Geology
Supervisor: Professor Maarten Felix
June 2020

Norwegian University of Science and Technology
Faculty of Engineering
Department of Geoscience and Petroleum

NTNU
Norwegian University of
Science and Technology

Abstract

This project examines the organic-rich black shales from the Late Jurassic Spekk and Hekkingen Formation in two cores on the Norwegian shelf. Late Jurassic to Early Cretaceous organic-rich black shales were deposited on the Norwegian shelf during anoxic conditions. The study aims to detect astronomically forced cycles in black shales from the Late Jurassic using magnetic susceptibility data series and power spectral analysis, construct a stratigraphic time scale by dating the black shales using calibrated tuned astronomical time series based on Milankovitch cycles, and use the tuned time series for correlation of the cores. The cores are from the Froan Basin in the Møre-Trøndelag area of the Norwegian Sea (6307/07-U-03A), and from the Nordkapp Basin in the NE Barents Sea (7230/05-U-02). The cores were investigated by means of sedimentological description and measurements of magnetic susceptibility. The cores were logged on a 1:20 scale, and samples were taken every 5 cm in an interval of ~20 m in the cores. Magnetic susceptibility was measured using a Kappabridge MFK1-A instrument. Power spectral analysis and estimation of sedimentation in the data series were conducted to identify cyclicities in the black shales related to Milankovitch cycles.

Based on the sedimentological description, the sediments were separated into six facies: (1) laminated black shale, (2) iron-rich black shale, (3) muddy sandstone, (4) carbonate cemented shale, (5) glauconite bedded shale, and (6) massive sandstone. The laminated black shale facies dominate the Late Jurassic deposits in the cores, with iron-rich black shale beds in evenly spaced intervals within the laminated black shale. The highest average magnetic susceptibility values were measured in the iron-rich black shale beds. The logged intervals in the two cores have an overall coarsening upward sequence, with silty and sandy black shales, muddy sandstones, and massive sandstone facies in the upper parts of the cores associated with the lowest average magnetic susceptibility measurements.

The power spectral analysis was performed on the magnetic susceptibility measurements and revealed several significant cycles. Ratios between the cycle lengths corresponds to ratios between Milankovitch cycles of long and short eccentricity, obliquity, and precession. Changes in the dominant frequencies throughout the core suggest a variation in sedimentation rates. The average sedimentation rates for the cores were estimated by amplitude modulation and expected ratios of Milankovitch cycles. The estimated average sedimentation rate of the core from the Froan Basin in the Norwegian Sea is 1.19 cm/ka with a variation between 1.15 cm/ka to 1.64 cm/ka, leading to a total duration of 1.67 Ma for the 19.8 m section. Astrochronology calibrated with the tuned astronomical time series from the Milankovitch cycles correlated to radiometric dates from the literature generates an age between 157.70 ±1.3 Ma and 156.03 ±1.3 Ma in the 19.8 m section from the base of the black shale formation, corresponding to a Late Oxfordian to Early Kimmeridgian age. In the core from the Nordkapp Basin in the Barents Sea, the average sedimentation rate is 1.14 cm/ka with a variation between 0.84 cm/ka to 1.81 cm/ka, leading to a total duration of the 18.9 m section of 1.68 Ma. The age is between

157.70 ±1.3 Ma and 156.02 ±1.3 Ma in the 18.9 m section from the base of the shale formation, corresponding to a Late Oxfordian to Early Kimmeridgian age.

Sammendrag

Dette prosjektet undersøker de organisk rike svartskifrene fra Sen Jura fra Spekk og Hekkingen Formasjonene i to kjerner på norsk sokkel. Sen Jura til Tidlig Kritt organisk rik svartskifer ble avsatt på norsk sokkel under anoksiske forhold. Studiet tar sikte på å oppdage astronomisk genererte sykluser i svarte skifer fra Sen Jura ved bruk av magnetiske susceptibilitet og effektspektrumanalyse, konstruere en stratigrafisk tidsskala ved datering av de svarte skifrene ved hjelp av kalibrerte astronomiske tidsserier basert på Milankovitch-sykluser og bruke de innstilte tidsseriene for korrelasjon av kjernene. Kjernene er fra Froanbassenget i Møre-Trøndelag-området i Norskehavet (6307/07-U-03A), og fra Nordkappbassenget i det nordøstlige Barentshavet (7230/05-U-02). Kjernene ble undersøkt ved hjelp av sedimentologisk beskrivelse og målinger av magnetisk susceptibilitet. Kjernene ble logget i en skala fra 1:20, og prøver ble tatt hver 5 cm i et intervall på ~20 m i kjernene. Magnetisk susceptibilitet ble målt ved bruk av et Kappabridge MFK1-A instrument. Effektspektrumanalyse og estimering av sedimentasjon i dataserien ble utført for å identifisere sykluser i svartskiferen relatert til Milankovitch-sykluser.

Basert på den sedimentologiske beskrivelsen, ble sedimentene separert i seks facies: (1) laminert svart skifer, (2) jernrik svart skifer, (3) siltig- og leirrik sandstein, (4) karbonat-sementert skifer, (5) glaukonitt lagdelt skifer, og (6) massiv sandstein. De laminerte svartskifer facies dominerer de sene juraforekomstene i kjernene, med jernrike sorte skiferlag i jevn distanse mellom den laminerte svartskiferen. De høyeste gjennomsnittlige magnetiske susceptibilitetsmålingene ble målt i de jernrike sort skiferlagene. De loggede intervallene i de to kjernene har en generell oppovergrovende sekvens, med siltige og sandete svartskifer, siltig- og leirrik sandsteiner og massive sandsteins facier i de øvre delene av kjernene assosiert med de laveste gjennomsnittlige magnetiske susceptibilitetsmålingene.

Effektspektrumanalyse ble utført på målinger av magnetisk susceptibilitet og avdekket flere signifikante sykluser. Forholdet mellom sykluslengdene tilsvarer forholdet mellom Milankovitch-syklusene med lang og kort eksentrisitet, oblikvitet og presesjon. Endringer i de dominerende frekvensene gjennom kjernen antyder en variasjon i sedimentasjonsgraden. Gjennomsnittlig sedimentasjonshastighet for kjernene ble estimert ved amplitude-modulasjon og forventede forhold mellom Milankovitch-sykluser. Den estimerte gjennomsnittlige sedimentasjonshastigheten for kjernen fra Froanbassenget i Norskehavet er 1.19 cm/årtusen med en variasjon mellom 1.15 cm/årtusen til 1.64 cm/årtusen, noe som fører til en total varighet på 1.67 millioner år for seksjonen på 19.8 m. Astrokronologi kalibrert med den innstilte astronomiske tidsserien fra Milankovitch-syklusene korrelert med radiometriske datoer fra litteraturen genererer en alder mellom 157.70 ± 1.3 og 156.03 ± 1.3 millioner år i seksjonen på 19.8 m fra starten av svartskiferdannelsen, tilsvarende en Sent Oxfordian til tidlig Kimmeridgian alder. I kjernen fra Nordkappbassenget i Barentshavet er gjennomsnittlig sedimentasjonshastighet 1.29 cm/årtusen med en variasjon mellom 1.26 cm/årtusen til 1.35 cm/årtusen, noe som fører til en total varighet i den 18.9 m seksjonen på 1.68 millioner år. Alderen er mellom 157.70 ± 1.3 og

156.02 ± 1.3 millioner år i den 18.9 m lange seksjonen fra skiferformasjonen, tilsvarende en Sen Oxfordian til Tidlig Kimmeridgian alder.

Acknowledgments

This thesis is part of a Master of Science in Geology with a specialization in Arctic Geology, at the Department of Geoscience and Petroleum, Norwegian University of Science and Technology (NTNU), Trondheim, Norway.

First, I would like to thank my supervisor Professor Maarten Felix for the guidance throughout this work and help in proofreading my drafts. Thank you also for the great fieldwork in France. I learn a lot about sedimentology and “reading” the landscape on that trip.

I would also like to thank Nathan Church and Professor Karl Fabian at the Department of Geoscience and Petroleum with help on the lab work and the magnetic measurements, and a special thanks to Nathan Church for all the discussions during my work. Thank you also to Atle Mørk for giving me access to the core storage facility at Dora were the logging and sampling took place and fellow Master student Maren Hope Blå for the support during the logging at Dora.

Finally, I wish to thank friends and family for their great support and patience when writing my master's thesis.

Table of Contents

List of Figures

List of Tables

1. Introduction

The depositional environment on the Norwegian shelf during the Late Jurassic to Early Cretaceous was that of a closed to restricted marine system with anoxic to dysoxic bottom waters, providing the conditions for deposition of black shales in deep marine settings (Hamar et al., 1983; Loseth and Tveten, 1996; Smelror et al., 2001; Bugge et al., 2002; Langrock et al., 2003). The restricted conditions on the Norwegian shelf, and warm and humid climate during the Late Jurassic Period lead to unusually high accumulation and preservation of organic carbon in the sediments (Langrock et al., 2003; Mutterlose et al., 2003). The organic-rich black shales of the time equivalent Spekk and Hekkingen Formations were deposited during the Late Oxfordian/Early Kimmeridgian to Ryazanian age (Dalland et al., 1988).

Climate control on sediment yield and the depositional environment are well established (Langbein and Schumm, 1958; Pederson et al., 2000; Collins and Bras, 2008). Global climatic change is controlled by astronomical forcing due to variation in insolation (Berger, 1988; Boulila et al., 2010). The analysis of the global signal recorded by Earth's astronomical forcing of insolation on the climate of the past in sedimentary deposits is called cyclostratigraphy (Hinnov, 2013). Many cyclostratigraphic studies have discovered cyclicities in sediments associated with astronomical forcing of the climate (Boulila et al., 2010). One way of determining the signal of the climate-induced cyclicities is by applying rock magnetic cyclostratigraphy to a sedimentary sequence (Kodama and Hinnov, 2014; Kodama, 2019). Deep marine mudstones tend to be more stratigraphically complete than coarser-grained siliciclastic successions from shallow marine environments, making them excellent sediments to perform cyclostratigraphic analysis on (Weedon et al., 1999). Therefore, cyclostratigraphy has been used numerous times on marine mudstones. Weedon et al. (1999) and Weedon et al. (2004) performed cyclostratigraphic analysis on the rhythmic beds of the Kimmeridge Clay Formation using magnetic susceptibility and found cycles in the Milankovitch band associated with astronomical forcing. Huang et al. (2010) also found Milankovitch cycles when they investigated the Kimmeridge Clay Formation using total organic carbon (TOC) and a formation microscanner. Qvam (2018) investigated the Kimmeridge Clay Formation time equivalent Hekkingen Formation in the Barents Sea with magnetic susceptibility and found cycles corresponding to Milankovitch cycles. Mutterlose et al. (2003) observed three main types of bedding cycles in cores from the Late Jurassic to Early Cretaceous. The cycles were related to the changes in the sedimentation caused by fluctuations in (1) carbonate productivity, (2) siderite/dolomite concretions in the black shale, and (3) clastic input of silts in the mudstone. All cycles were controlled by eccentricity and obliquity cycles. The cycles from the siderite/dolomite concretions, and the clastic input were influenced by the precession cycles.

In this study a ~20 m section of organic-rich black shales from cores in the Norwegian Sea and the Barents Sea was sampled. The samples were measured by magnetic susceptibility for analysis of potential Milankovitch cycles using power spectral analysis. Analysis of sedimentation rates was performed to construct a tuned time

series to date the black shales creating a stratigraphic time scale for the black shales in the Norwegian and Barents Sea.

The two cores used in this study were drilled in the Spekk Formation from the Froan Basin in the Møre-Trøndelag area of the Norwegian Sea (6307/07-U-03A), and in the Hekkingen Formation from the Nordkapp Basin of the NE Barents Sea (7230/05-U-02) during the shallow stratigraphic drilling program (Rise and Sættem, 1994). Biostratigraphy from the ammonite succession in core 7230/05-U-02 (Wierzbowski and Smelror, 1993), and calculated sedimentation rates for different bedding cycles by Mutterlose et al. (2003) provide a constraint on the sedimentation rates allowing for more robust identification of Milankovitch cycles. A 64 m section of the Spekk Formation in core 6307/07-U-03A and a 20 m section of the Hekkingen Formation were logged and divided into facies to determine the optimal place for magnetic susceptibility measurements and to investigate the relationship between the depositional changes and magnetic measurements. In each core, an ~20 m section was sampled for the magnetic susceptibility measurements.

This study aims were to (1) detect astronomically forced climate cycles in black shales from the Late Jurassic using magnetic susceptibility data series and power spectral analysis, (2) construct a stratigraphic time scale by dating the black shales using calibrated tuned astronomical time series based on Milankovitch cycles, (3) and use the tuned time series for correlation of the cores.

2. Theory

2.1. Cyclostratigraphy and Milankovitch cycles

Cyclostratigraphy is the analysis of global signals recorded by Earth's astronomical forcing of insolation on the climate of the past in sedimentary deposits (Hinnov, 2013). The method of cyclostratigraphy is largely based on the work of Milankovitch. Milankovitch studied the driving effects of Earth's climate by the movement of the Sun and objects in the solar system. The Astronomical Theory of paleoclimate as it is known today has its origin in the beginning of the nineteenth century, with many researchers contributing to the evolution of the idea (Berger, 2012). The purpose of the theory is to explain the variation in climate that occurs in quasiperiodic times in the orders of tens to hundreds of thousands of years (Berger, 2012; Hinnov, 2013). The variation in climate will change temperature and precipitation which controls the atmospheric and oceanic circulation patterns on earth (Swientek, 2002). The feedback from the circulation patterns result in changes in the organic and carbonate matter productivity, changes in the redox conditions, and fluxes in clastic input controlled by erosion in the hinterland (Swientek, 2002). The distribution of solar insolation which Earth receives varies with the seasons and latitudes. The astronomical parameters determining the insolation received at the Earth's surface are: (1) The *Earth's orbital eccentricity* (*e),* which is the changing Earth-Sun distance in the orbit of the Earth around the Sun which governs the total insolation received at the Earth's surface, (2) *the obliquity* (ε), which is the inclination of the rotational axis of the Earth, the tilt changes the latitudinal insolation, and (3) *the precession of Earth's rotation axis* (ψ), controlling the timing and locations of the seasons related to Earth's orbit (Hinnov, 2013).

The main eccentricity terms are the 405-ka, 124-ka, and 95-ka periods (Laskar et al., 2004). The average obliquity periodicity is 41-ka, and the average precessional period is 21,740 years, but the period has a broad range (Berger, 1976).

The first significant evidence for climate change induced by astronomical forcing came from the oceanic record (Hinnov, 2013). Analysis of deep-sea drilled cores by Hays et al. (1976) showed the 100-ka, 41-ka, 23-ka, and 19-ka quasiperiodic cycles connected to the Earth's eccentricity, obliquity and precession in the sedimentary record for the first time (Berger, 2012). Around the same time astronomical models of the planetary system showed the same periods (e.g. Berger, 1978), confirming the astronomical periods in the sedimentary record. Astronomical models have in later years evolved from analytical to more detailed numerical solutions calculated by computers (e.g.Laskar et al., 2004), giving a more accurate picture of the evolution of orbital cycles and the chaotic behaviour of the solar system (Hinnov, 2013).

The orbital cycles in the solar system have not been stable over geological periods. The evolution in orbital cycles complicates the calculation of cycles over large time frames. Laskar et al. (2004) calculated numerical solutions for the solar system hundreds of millions of years in the past, showing the chaotic evolution and

complex modulation on astronomical parameters (Hinnov, 2013; Zeebe & Lourens, 2019). The evolution in the Earth's orbital motion and orientation of the Earth spin axis is caused by the gravitational disturbance from other objects like planets in the solar system (Laskar et al., 2004). Accurate astronomical time scales later than ~50 Ma have yet to be constructed, due to the conflicting orbital calculations (Zeebe & Lourens, 2019). The orbital cycles can be characterised as quasiperiodic over a timespan of a few million years, but the chaotic diffusion over vast periods (e.g. 150 Ma) makes this inference impossible (Olsen et al., 2019). However, the 405-ka term has been calculated to be very stable over the Mesozoic time scale, and can be used for tuning of the time scale in the Mesozoic (Laskar et al., 2004). The major astronomical periods from the Late Jurassic Period (150 Ma) are given in Table 1. All the periods are based on estimation except the 405 ka term, which was calculated by Laskar et al. (2004). Waltham (2015) calculated and estimated the uncertainties in obliquity and precession periods over geological time, and the periods and uncertainties of the eccentricity cycle in present times. The periods and uncertainties in the eccentricity cycle could be different in the Late Jurassic Period, however, the eccentricity cycles (particularly the 405 ka period) are relatively stable throughout geological times, so the uncertainties have not change considerably.

Table 1. *The main astronomical periods from 150 Ma (Late Jurassic). The eccentricity periods and uncertainties are taken from Waltham (2015) and is based on the present day periods. Obliquity and precession periods from 150 Ma (Late Jurassic), including uncertainty are taken from calculation made by Waltham (2015).*

Astronomical cycle	Period (ka)	Uncertainty (±ka)	Uncertainty (%)
Long Eccentricity	405.60	2.4	0.6
Short Eccentricity	123.90	2.6	2.1
Short Eccentricity	94.90	1.4	1.5
Main Obliquity Period	38.00	1.7	4.5
Earth Axis Precession Period	24.48	0.68	2.8
Climatic Precession Period	22.65	0.58	2.6
Climatic Precession Period	21.46	0.53	2.5
Climatic Precession Period	18.43	0.44	2.4
Climatic Precession Period	18.29	0.43	2.4

3. Geological Setting

The geological setting gives a brief overview of the depositional environment at the time of deposition, geological structures, processes through time in the project areas, sedimentation rates in the project areas, and description of the cores. The continuity of the depositional environment on the Norwegian shelf led to similar depositional environments in all project areas.

3.1. Geological History of the Project Areas

Froan Basin in the Møre-Trøndelag area of the Norwegian Sea

The Norwegian Sea is a rifted passive continental margin located between 62°N and 69°30'N on the Norwegian continental shelf (Blystad, 1995). Blystad (1995) separated the formation of the Norwegian Sea into three major events: (1) Closure of the Iapetus Ocean related to the Caledonian Orogeny in the Late Silurian to Early Devonian, (2) extensional deformation events leading to the separation of Greenland and Eurasia in the Late Devonian to Palaeocene, and (3) active seafloor spreading between Eurasia and Greenland in the North Atlantic in the Early Eocene to present.

Part of the Norwegian Sea was subjected to rifting during the late Permian/Early Triassic, leading to the formation of rotated fault blocks. The faulting provided accommodation space for deposition of thick layers of Triassic sediments in a fluvial sabkha environment. During the Early to Middle Jurassic, the basins in the Norwegian Sea subsided with sediments infilling by a deltaic to fluvial system. The Norwegian Sea experienced major rifting events lasting from the late Middle Jurassic until the Early Cretaceous (Blystad, 1995).

The Trøndelag Platform was created during the late Middle Jurassic to Early Cretaceous rifting event (Brekke and Riis, 1987; Blystad, 1995). The platform has an area of more than 50 000 km^2 and was formally defined by Gabrielsen et al. (1984) (Figure 1). The area was subjected to many rifting and basin creation episodes before the Cretaceous (Brekke and Riis, 1987).

The Froan Basin is part of the Trøndelag Platform (Figure 1); the basin is elongated and about 250 km long and 50 km wide at its widest (Blystad, 1995). The basin consists of half grabens. In the South, the basin is limited by the boundary fault along the Frøya High. The Froan Basin was formed during a late Early Permian rifting event, creating a landscape of faulted blocks (Brekke and Riis, 1987; Blystad, 1995).

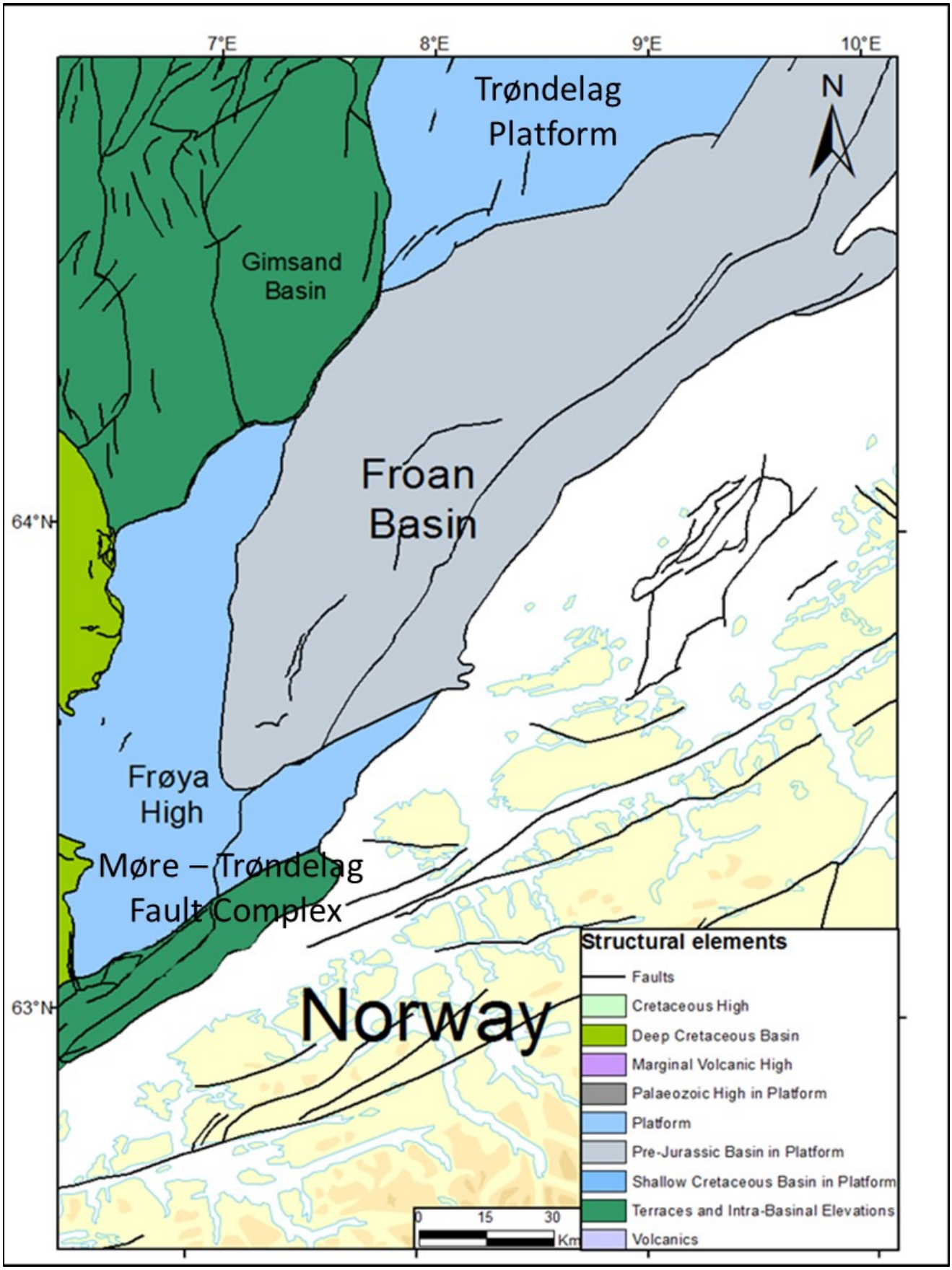

Figure 1. *Structural map of the Froan Basin and the surrounding areas in the Norwegian Sea. Modified from NPD (2019).*

The Nordkapp Basin in the Barents Sea

The Barents Sea consists of a vast epicontinental sea surrounded by passive continental margins in the west and north. In the north are the Svalbard islands and Franz Josef Land, in the east Novaya Zemlya and to the south the Kola peninsula and Norwegian coast (Faleide et al., 1984). The Barents Sea can be divided into an eastern and western part by an N-S trending monocline structure. The geology of the western region reflects a complex tectonic history, with a mosaic of basins, platforms, and structural highs related to tectonic processes along the western and north-western edges of the Eurasian plate (Worsley, 2008).

The late Devonian to middle Permian (385-270Ma) is characterized by rifting, followed by the Caledonian Svalbardian compressing movements, followed by the creation of post-rift carbonate platforms. In this period from the late Devonian to the Early Carboniferous, the Nordkapp Basin in the South Western Barents Sea was formed (Bugge et al., 2002; Worsley, 2008).

The Nordkapp Basin is an ENE-WSW trending sub-basin dominated by salt diapirs (Figure 2). The areal extent is around 23 000 km^3 (Faleide et al., 1984; Bugge et al., 2002). The basin formed during the Late Palaeozoic rifting and regional extension (Bugge et al., 2002). Coaly alluvial siliciclastics were deposited in the basin initially. In the Mid Carboniferous, the area experienced renewed rifting and a more arid climate, conglomerates and evaporites were deposited in the lower part of the basin and coarse red beds in the margins (Nøttvedt et al., 1993). In the Permian, carbonates, siliciclastics and chert were deposited in the basin. Sediments were supplied from the south and east during the Early and Middle Triassic. At the time, shallow marine environments dominated the area (Nøttvedt et al., 1993). The environment in the Nordkapp Basin from the Early Triassic to Late Cretaceous alternated between marine basin and shelf to coastal and delta plain (Bugge et al., 2002). Black shales were deposited during the Late Oxfordian to Lower Volgian in the Hekkingen Formation. The basin was at the time deeper than the surrounding platform area, comprising of many smaller sub-basins.

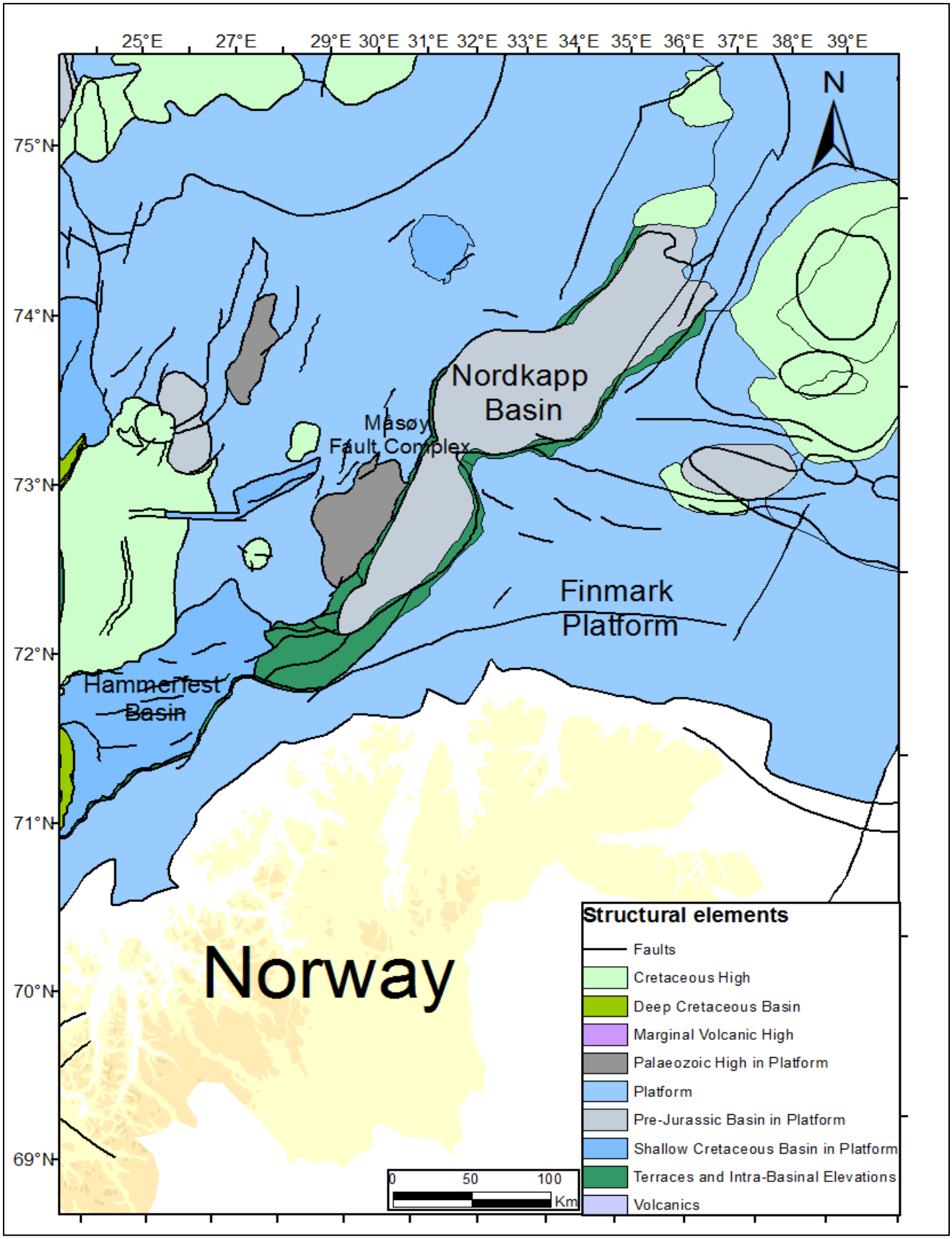

Figure 2. *Structural map of the Nordkapp Basin and the surrounding areas in the Barents Sea. Modified from NPD (2019).*

3.2. Depositional Environment

The North Atlantic experienced low seafloor spreading rates during the Late Jurassic to Early Cretaceous. A regional sea-level low stand in the Late Jurassic Period created a marine environment with restricted basins. The restricted environment led to the deposition and formation of anoxic black shales in the Norwegian-Greenland Seaway (Smelror et al., 2001; Langrock et al., 2003; Mutterlose et al., 2003). Indications of suboxic to anoxic bottom water conditions come from the formation of autochthonous pyrite framboids and well-developed lamination. A mix of terrigenous and marine organic content suggests deposition in a shelf environment (Langrock et al., 2003; Mutterlose et al., 2003). The restricted conditions in the seaway and warm and humid climate during the low stand led to unusually high accumulation and preservation of organic carbon in the sediments, with preservation being the primary control on the formation of the black shale (Langrock et al., 2003; Mutterlose et al., 2003). Siderite-rich beds found in the black shales may have formed in early diagenetic processes under marine conditions, possibly related to degradation reactions of organic content (Mørk et al., 2002).

3.3. Sedimentation Rates

To convert the data series from the cyclostratigraphic analysis from the depth to time domain, sedimentation rates are needed. Sedimentation rates on the Norwegian shelf in the Late Jurassic Period varied significantly. Mutterlose et al. (2003) estimated several sedimentation rates based on biostratigraphy and astronomical analysis of spectrograms for three types of cyclic behaviour in the Greenland-Norway seaway in the Late Jurassic to Early Cretaceous (Table 2). Type A and B cycles were produced by varying sedimentation conditions caused by fluctuations of carbonate productivity and redox regime. Type A cycles were caused by variation in the carbonate content and the bioturbation pattern, and type B is related to an alternation between black shale and siderite/dolomite concretions. Type C cycles are described as an alternation between black shales and silt laminae; in this period the depositional environment was characterised by clastic impulses controlled by astronomical forcing (Mutterlose et al., 2003). All the cycle types were observed in core 6307/07-U-02, which is drilled ~2 km from core 6307/07-U-03A. Assuming the lateral changes in the basin are not too high, the sedimentation rates are likely to be similar in core 6307/07-U-03A.

Georgiev et al. (2017) calculated sedimentation rates for core 7230/05-U-02 from Re-Os isochron measurements in the anoxic black shales deposited in the Late Jurassic–Early Cretaceous. The sedimentation rates estimated for the Nordkapp Basin were ~5.0 m/Ma for the Alge Member and ~1.3 m/Ma for the Krill Member, suggesting lower sedimentation rates than Mutterlose et al. (2003) estimated for the Volgian stage (Late Jurassic – Early Cretaceous).

Table 2. *Different estimates of sedimentation rates (SR) . Modified from Mutterlose et al. (2003)*

Cycle type	Biostratigraphic SR, m/Ma	Astronomical SR, m/Ma
Type A (early Valanginian)	3.8 ± 0.8	4.4 ± 0.2
Type B (late Volgian)	19.0 ± 7.6	16.2 ± 0.4
Type C (early Volgian)	6.7 ± 2.5	8.2 ± 0.4

3.4. Description of Cores

Between 1988 and 1992, a shallow stratigraphic drilling program was undertaken by the Continental Shelf Institute (Rise and Sættem, 1994). Two of the cores drilled in this program were analysed in this project. The cores were drilled in the Froan Basin located in the Møre-Trøndelag area of the Norwegian Sea (6307/07-U-03A) and the Nordkapp Basin in the Barents Sea (7230/05-U-02). The stratigraphic formations with their main lithologies in the Norwegian Sea and the Barents Sea are shown in Figure 3. The black shale deposits from the Late Jurassic in the Norwegian Sea corresponds to the Spekk Formation, and the black shales from the Barents Sea corresponds to the Hekkingen Formation. The Spekk and Hekkingen Formations were deposited in the Late Jurassic – Early Cretaceous (Mørk et al., 2003).

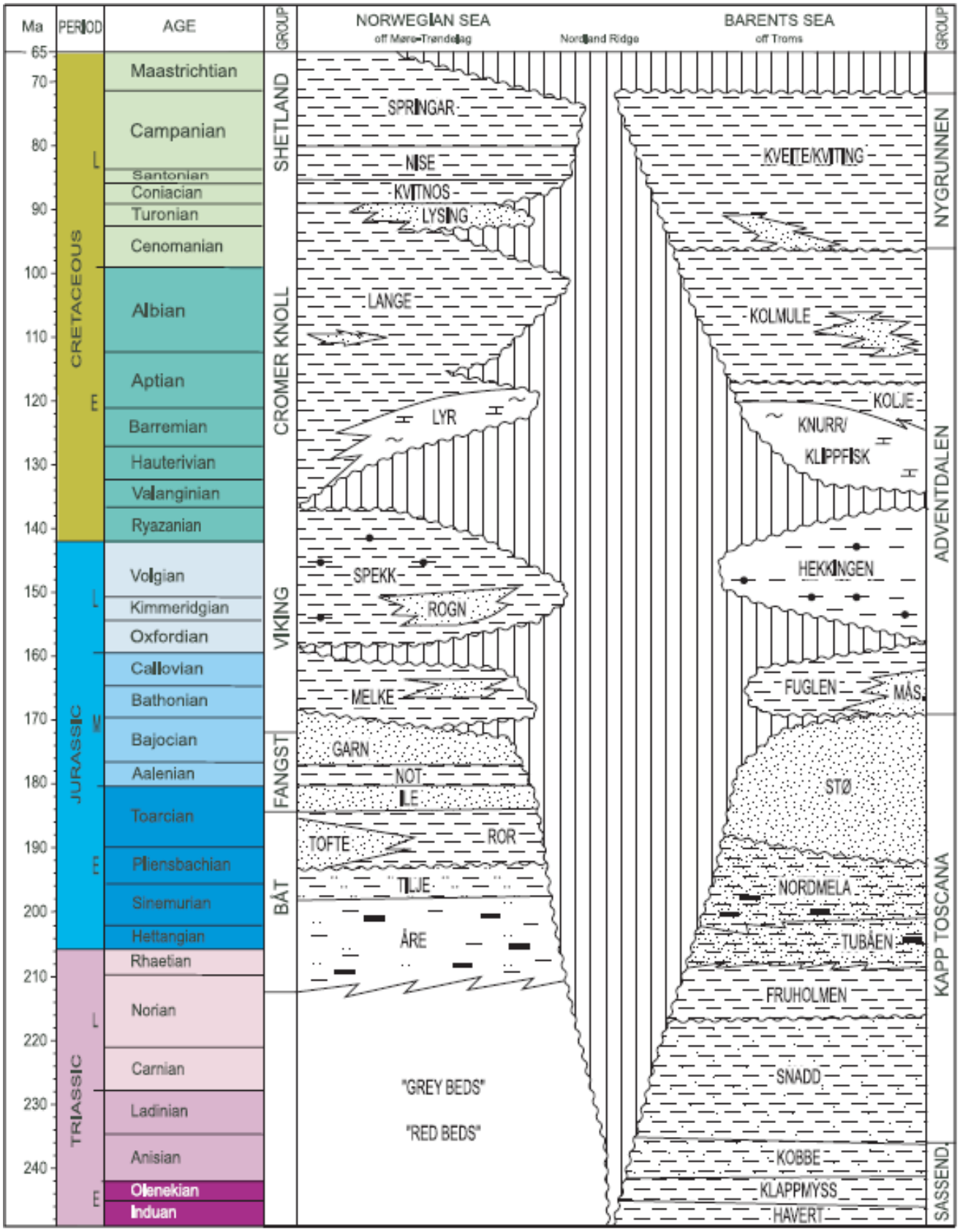

Figure 3. *Stratigraphic formations in the Norwegian and Barents Sea. The Spekk Formation was deposited in the Norwegian Sea, and the Hekkingen Formation was deposited in the Barents Sea during the Late Jurassic. From Mørk et al. (2003).*

Core 6307/07-U-03A was drilled in the southern parts of the Froan Basin in the Møre-Trøndelag area of the Norwegian Sea (Figure 4) (Mørk and Johnsen, 2005). The black shale section is at a depth of 81-16 metres in the core. Late Jurassic to Early Cretaceous sediments were cored, with the organic-rich black shales from the Late Jurassic – Early Cretaceous Spekk Formation and sandstones from the Rogn Formation overlain by the Lower Cretaceous Lange Formation (Mørk et al., 2003). The Spekk Formation is deposits of Oxfordian to Ryazanian age in an marine anoxic bottom water conditions (Dalland et al., 1988). The Spekk Formation is dominated by smectite/mixed-layer clay (Mørk et al., 2003). The total organic content of the black shale deposited during the Volgian Period (Late Jurassic) in the neighbouring core 6307/07-U-02 is between 3.9 and 4.3 wt% (Langrock et al., 2003). Assuming the lateral changes between the cores is small, a similar organic content can be expected in core 6307/07-U-03A. The palaeolatitude of the sites during the Late Jurassic was 43°N according to reconstructions by Mutterlose et al. (2003).

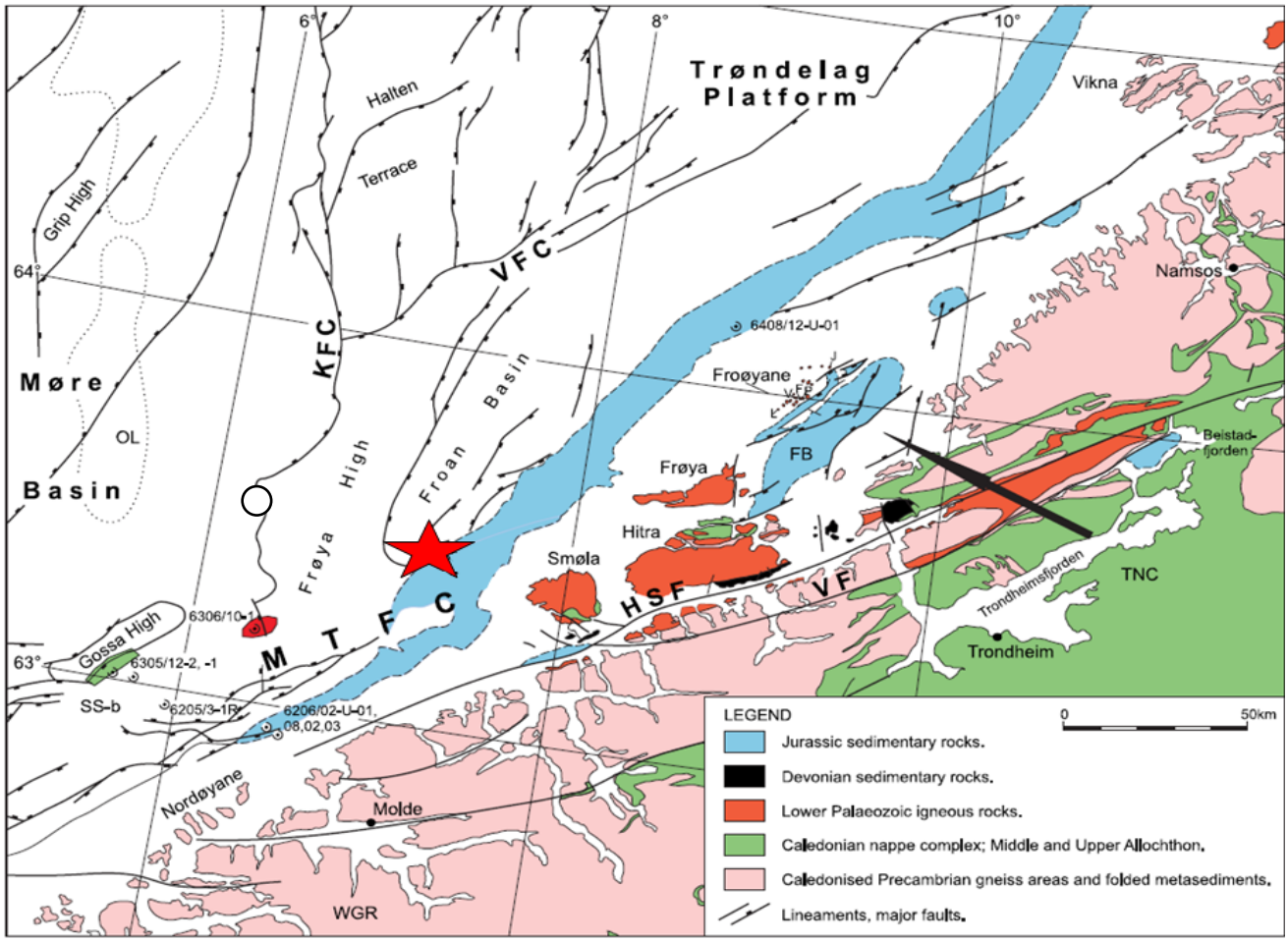

Figure 4. *Map of the main geological provinces and structural elements in the Møre-Trøndelag area of the Norwegian Sea. FB: Frohavet Basin, WGR: Western Gneiss Region, VFC: Vingleia Fault Complex, VF: Vingleia Fault, SS-b: Slørebotn Sub-basin, TNC: Trondheim Nappe Complex, MTFC: Møre-Trøndelag Fault Complex, KFC: Klakk Fault Complex, HSF: Hitra-Snåsa Fault. Core 6307/07-U-03A is indicated with a red star on the map. From Mørk and Johnsen (2005).*

Core 7230/05-U-02 was drilled in the central part of the Nordkapp Basin in the Barents Sea (Figure 5). The core length is 95.1 m (Bugge et al., 2002). The bottom part of the core consists of deltaic sediments with coarsening upward sandstone mouth bar complexes and fining upward sandstone distributary channel complexes of the Middle Stø Formation overlain by bioturbated, glauconitic sandstones of the Upper Stø Formation (Bugge et al., 2002). The silty shales of the Fuglen Formation are abruptly overlain by Late Oxfordian to Late Kimmeridgian black shales of the Hekkingen Formation (Bugge et al., 2002). The black shales of the Hekkingen Formation are around 20 metres thick, from 52 m to 32 m depth in the core, with a sharp and erosive contact to the underling silty Fuglen Formation (Bugge et al., 2002). A 10 cm thick layer with glauconitic shale clasts is present in the contact zone. The black shales of the Hekkingen Formation consist of paper shale with laminae of silt and skeletal fragments. Pyrite laminae and concretions are also common in the core. The cored section corresponds to the Alge Member of the Hekkingen Formation defined by Dalland et al. (1988), the Alge Member is associated with higher radioactivity and total organic carbon (TOC) than the Krill Member (Bugge et al., 2002). Georgiev et al. (2017) dated the algae member to ~157.7 ±1.3 Ma to ~154.7 ±1.1 Ma. Georgiev et al. (2017) measured the TOC in the Alge Member to be between 10.10 and 17.62 wt %, and Bugge et al. (2002) measured the TOC to be ranging from 7 to 23 wt% in the core. The Alge Member terminated against the overlying Krill Member of the Hekkingen Formation at ~ 34.60 m depth in core 7230/05-U-02 according to Georgiev et al. (2017). The palaeolatitude of the sites during the Late Jurassic was ~53°N according to reconstructions by Mutterlose et al. (2003).

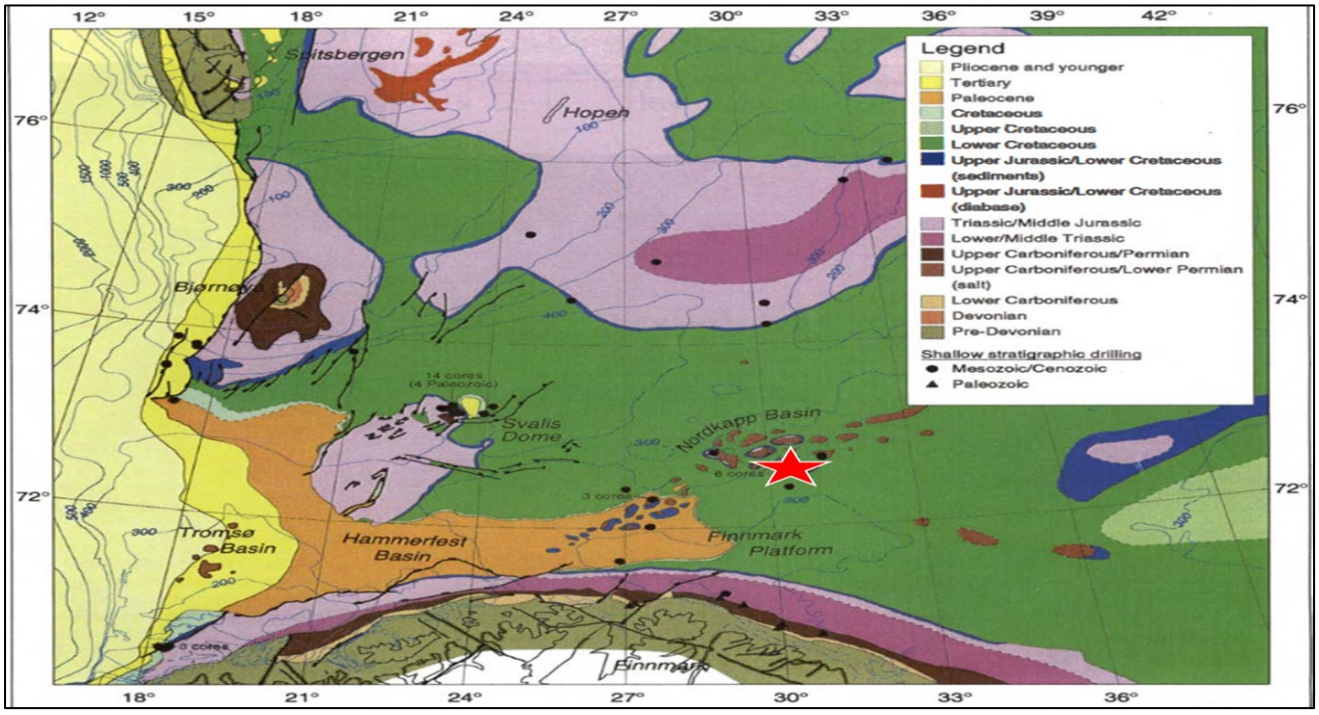

Figure 5. *Map of the main geological provinces and structural elements in the Barents shelf. Core 7230/05-U-02 is indicated with a red star. From Bugge et al. (1995).*

4. Methods

4.1. Logging of Core

Logging of cores on a scale of 1:20 took place at the core storage facility at Dora in Trondheim. A 64 m section of the Spekk Formation in core 6307/07-U-03A, and a 20 m section of the Hekkingen Formation was logged. The cores were described using a handheld lens and a microscope. The sedimentary description focused on characteristics like sedimentary structures, lithology, colour, and grain size. Different facies were defined based on the sedimentary description. The cores are made up of two halves, one display half and one working half which can be sampled. The logging was based on both core halves, since the core used for presentation is covered in a varnish, which can make the sedimentary structures hard to detect and distinguish. Some of the spotty varnish features can be mistaken for sedimentary structures, if not carefully observed with a hand lens. The other half of the core used for sampling does not have varnish, so the core used for sampling was used to compare with the varnished half of the core. The computer program SedLog 3.0 (Zervas et al., 2009) was used to create digital images of the sedimentary logs.

4.2. Magnetic Susceptibility

Three hundred and sixty-one and three hundred and sixty-three un-oriented samples were taken from core 6307/07-U-03A and 7230/05-U-02, respectively. The sample were taken from between 59.85 m to 79.65 m depth in core 6307/07-U-03A, and between 33.15 m to 52.05 m depth in core 7230/05-U-02. Samples were taken from core bits, and sawn to the correct sample size. The samples were taken every 5 cm in the half of the core used for sampling. The depths in the core half used for sampling were correlated with the other half of the core that had fixed depth control using laminae, beds, and sedimentological features that were recognized in both core halves. Some sections of the cores are hard to sample at the right depth due to reshuffling of material within the core box of the working-half cores. The reshuffling most likely happened under transport of the core boxes and affects the depth control used in further analysis; this results in uncertainties in the correlation of depths between the core halves. Gaps in the working half of the core led to unregular sampling distances in some parts of the core. The samples were normalized by weight and the magnetic susceptibility (χ) measured in room temperature with a Multi-Function Kappabridge MFK1-A instrument, the sample was placed in a 44 cm^3 plastic cylinder. The measurements were repeated three times, and the average value of magnetic susceptibility was used.

Magnetic susceptibility is the magnetization of a material when subjected to a small external magnetic field (Boulila et al., 2010). Ferromagnetic iron oxides like magnetite and maghemite have a strong positive magnetic susceptibility, clays and pyrite are paramagnetic with weak positive magnetic susceptibility, and calcium carbonate and quartz are diamagnetic with very weak negative magnetic susceptibility.

The spacing between the samples in the magnetic susceptibility measurements was based on the sediment accumulation rate (SAR) and the smallest target frequency. The target frequencies are based on Milankovitch periods (Table 1). The Nyquist frequency determines the smallest frequencies that can be detected and are based on the sampling spacing (Kodama, 2019):

$$Nyquist\ frequency\ = 1/(2 * sample\ spacing) \quad (1)$$

Based on the calculations from Georgiev et al. (2017), the sedimentation rate for core 7230/05-U-02 in the Alge member is ~0.5 cm/ka. The shortest Milankovitch frequency is the processional cycle, which has a periodicity of ~20 ka. Eq. 1 yields a minimum sample spacing of 5 cm to find processional cycles with a sedimentation rate of ~0.5 cm/ka.

4.2. Spectral Analysis

Spectral analysis was performed with the package astrochron (Meyers, 2014) in R (R-CoreTeam, 2019). Because of gaps in the sequences, regular sampling intervals were obtained by linear interpolation of the data series. Outliers were removed to reduce the disproportionate influence of high susceptibility measurements, leading to concealment of the smaller variation throughout the sections. The outliers were removed by analysing the data points using a boxplot algorithm in astrochron. The boxplot and Q-Q plot before and after trimming for core 6307/07-U-03A are shown in Figure 6, no data point were removed from core 7230/05-U-02. The extent of the plot 'whiskers' extending from the box was decided by the coefficient of the whisker set to 1.5 times the length of the box. Outliers outside the wishers were removed. The data series were detrended to remove edge effects, the mean was subtracted from the data series, and zero-padded by the lowest power of two larger than the number of data points. Spectral analysis was conducted using the multi-taper method (MTM) of Thomson (1982). The time-bandwidth product was set to three in the MTM analysis. The harmonic f-test (Thomson, 1982) and LOWSPEC (Meyers, 2012) confidence levels are calculated in the MTM power spectrum. The confidence limit for the harmonic f-test and LOWSPEC used to judge the significance of the spectral peaks was

set to 90 %. An evolutive power spectral analysis was conducted on two of the data series, with a window length of 6 m, a step size of 1 m, with all other parameters the same as the MTM power spectra analysis.

The TimeOpt method (Meyers, 2015) was used for identification of the optimal average sedimentation rate for construction of the astrochronological time scale. The method combines amplitude modulation and frequency ratios using a probabilistic linear regression model, using an algorithm which identifies the sedimentation rate that simultaneously optimizes the eccentricity amplitude modulation of the precession band and the concentration of power at eccentricity and precession frequencies (Meyers, 2015). The method is independent of the method for identifying the significant power spectrum peaks. The amplitudes and phases of the eccentricity cycle is determined by modelling, this is beneficial because the amplitude and phases of the astronomical cycles are unconstrained in deep geological time (>50 Ma), contrary to the periods of the cycle (Meyers, 2015). Probable sedimentation rates between 0.44 cm/ka and 1.6 cm/ka were chosen as the sedimentation range in the analysis based on sedimentation rates in the area from the literature (Table 2). To investigate varying sedimentation rates, a template was included in the TimeOpt method. The template allows the evaluation of a wide range of variable sedimentation models, including. Differential accumulation across bedding couplets, linear accumulation rate change, step changes in sedimentation rate, and the presence of hiatuses.

A periodogram is used for estimation of spectral peaks for a stationary signal, but this standard method may lead to high variance. To reduce any variance, the signal is segmented and a periodogram is calculated for each segment, then averaging each periodogram. However, this method increases the bias of the spectral estimate. The multi-taper method (MTM) uses multiple orthogonal windows called Slepian windows, which provides optimal concentration of power within specific frequency bandwidth (Meyers, 2012) to compute multiple periodograms of the whole signal, then averaging the periodograms to construct the spectral estimate (Thomson, 1982; Xu et al., 1999). The MTM provides an optimal trade-off between frequency resolution, bias (accuracy), and consistency (precision) (Meyers, 2012). The Slepian window is used in the MTM to achieve minimum bias and variance. The Slepian window minimises variance by being orthogonal and optimally concentrated in frequency to minimise bias (Xu et al., 1999).

Robust locally-weighted regression spectral background estimation (LOWSPEC) was chosen because the conventional estimation for red noise is biased when the data contain a strong periodic signal, believed to be prevalent in cyclostratigraphic sequences (Meyers, 2012). The LOWSPEC model uses a median smoothing window to include fewer frequencies near the edges of the spectrum (Meyers, 2012). Limitations for cyclostratigraphic application include inflated confidence limit estimates (greater than expected false positive rate) and excessive clumping of false positives within the eccentricity band of the spectrum (Meyers, 2012). The LOWSPEC model achieves lower rates of false positive than the robust red noise commonly used in analysis (Meyers, 2012). The harmonic f-test is used to test for consistency in the phases of a sinusoidal in white and coloured noise (Thomson, 1982; Meyers, 2012). Astrochron identifies candidates for significant spectral

frequencies automatically based on the following criteria. The harmonic f-test and LOWSPEC modelling need to achieve the confidence level (e.g. 90%). Due to the smoothing inherent in the MTM power spectrum the frequencies will also be identified as significant if the confidence level of the LOWSPEC model is within ± half the power spectrum bandwidth resolution. In addition, to further reduce the false positive rate, the significant frequency must occur on a local power spectrum high, which is defined as occurring over the local LOWSPEC background estimate (Meyers, 2012). According to Meyers et al. (2001), the harmonic f-test is independent of the peaks' power, so the method can identify certain low-powered peaks to be statistically significant and may identify some high-power peaks as not statistically significant.

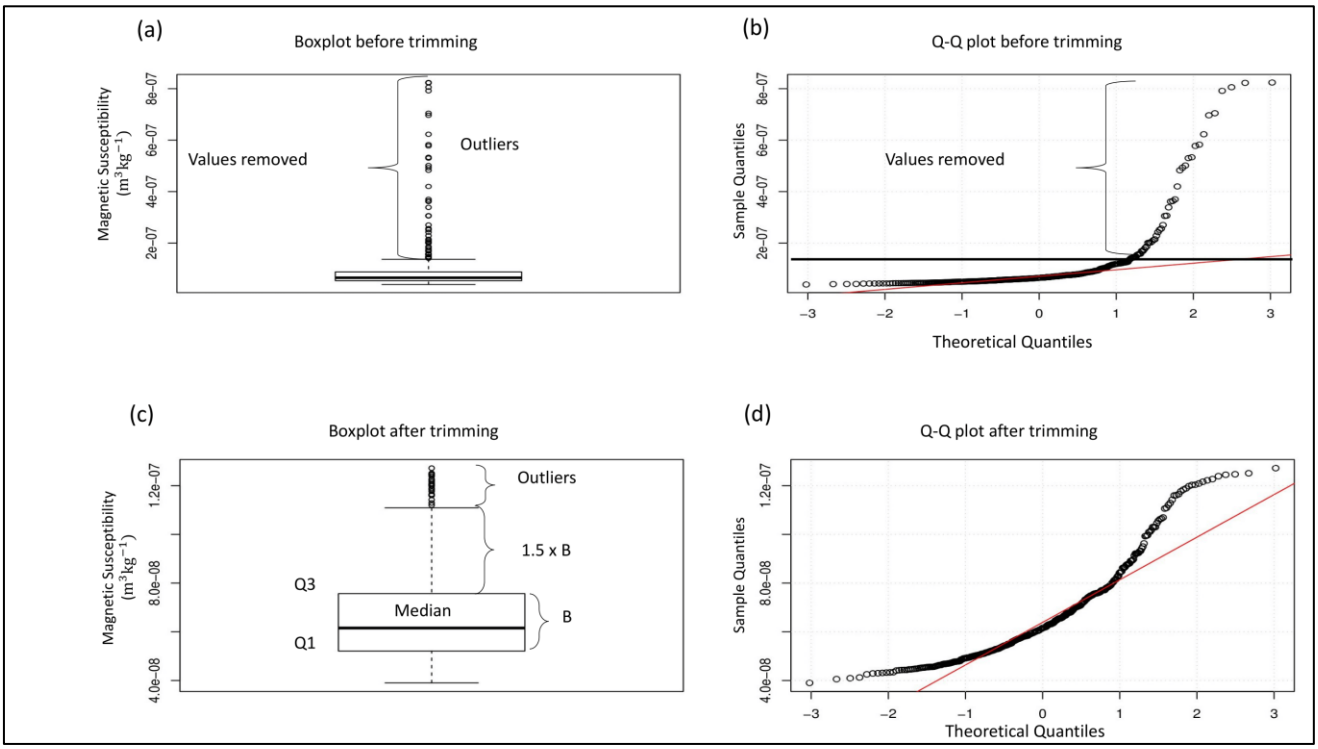

Figure 6. *Boxplots and Q-Q plots before and after the trimming of the magnetic susceptibility data series from core 6307/07-U-03A. (a) Boxplot before trimming, magnetic susceptibility values that are higher than the cut off values are removed (outliers). (b) The Q-Q plot before the trimming showing the quantiles of the magnetic susceptibility values as a function of theoretical quantiles with exponentially higher magnetic susceptibility values removed. (c) Boxplot after trimming showing the outliers, median value, Q1: first quartile (25 %) and Q3: third quartile (75 %), B: length of the box, and the coefficient for the whiskers set to 1.5. (d) Q-Q plot after trimming shows a more normally distributed data series.*

5. Results

5.1. Sedimentological Description

Based on sedimentological description of core 6307/07-U-03A and 7230/05-U-02, six facies are identified; (1) laminated black shales, (2) iron-rich black shale, (3) muddy sandstone, (4) carbonate cemented shale, (5) glauconite bedded shale, and (6) massive sandstone (Table 3 and Figure 7). Carbonate cemented shale, glauconite bedded shale, and massive sandstone facies are present only in a short section at one place in the cores, therefore, laminated black shales, iron-rich black shale, and muddy sandstone are the major facies identified.

Spekk Formation (Core 6307/07-U-03A)

The laminated black shale facies (Table 3) are the dominant facies in the Spekk Formation in core 6307/07-U-03A and makes up most of the logged section. Most of the lamination is horizontal planar lamination of clay-on-clay or silt-clay pairs, however, wavy cross-lamination and current ripple cross-lamination are also present in the logged section. Core 6307/07-U-03A contains a general upward coarsening sequence, with laminated black shale facies in the lower parts between ~80 m and ~29 m, and muddy sandstone (Table 3) in the upper parts of the core between ~29 m and 19 m changing into sandstones of the Rogn Formation in the uppermost metres of the logged core (Figure 8). The muddy sandstones show a chaotic texture of silt and sand sized sediments. The muddy sandstones found in the upper part of the core contain abundant mud clasts, and also bioturbation in some intervals (Table 3). Beds and laminae of siderite-rich black shales and siderite concretions (Table 3) are present within the laminated black shale at many places in the lower parts of the logged section. The siderite beds appear in roughly evenly spaced intervals with some gaps. The spacing is ~2 m in the lower parts of the section up to 70 m, ~4-5 m from 70 m to 60 m, and ~1-3 m from 60 m to 35 m in the black shale. The 0.7 m carbonate cemented shale interval around 42.5 m is heavily varnished (Table 3). Pyrite and siderite concretions/nodules are abundant throughout the core. Calcified fossil fragments can be found at several places in the logged section. The sediments show bioturbation in the middle part between 52 m and 45 m, and in the upper part between 22 m and 19 m in the core.

Hekkingen Formation (Core 7230/05-U-02)

Laminated black shale is the dominant facies throughout the logged section of the Hekkingen Formation in core 7230/05-U-02 (Table 3). The lamination is horizontal planar of mostly clay-on-clay pairs in the lower part

of the core, and lamination of clay-silt pairs in the upper part of the core. The core shows an overall upward coarsening pattern, with more silt and sandy shales in the upper parts of the core. The lowest part of the section between 52 m and 50 m contains a 10 cm bed with glauconite nodules up to 2 cm, with an erosive contact to the underlying section and a gradual contact to the overlying black shale. Beds, laminae, and concretions of pyrite-rich shales (Table 3) are present below 40 m (Figure 9). Calcified fossil fragments are abundant through the core, and a cone-in-cone structure is present at 36.0 m. The upper 2 m of the section have a more massive texture than the laminated shales in the rest of the core. The black shales in core 6307/07-U-03A have a greyer tone than the black shale in core 7230/05-U-02.

Interpretation

The black shales were deposited in an anoxic environment and have a high organic content due to a warm climate leading to high productivity (Smelror et al., 2001; Langrock et al., 2003; Mutterlose et al., 2003; Potter et al., 2005). The black shale was likely deposited from a combination of suspension settling and traction transport mechanisms. The clay and silt laminae pairs may have been created by pulses from dilute, low velocity turbidity currents, similar to what Boggs Jr and Boggs (2009) suggested for silt laminae pairs. Bioturbation can take place where the oxygen level is not too low, or the sediment deposits slowly (Potter et al., 2005), so bioturbation indicates more oxic conditions. The laminae may also stem from small-scale pulsed variation in disseminated organic matter, possibly connected to climate cycles, or cycles of oxygenation events in the bottom water of the basin, as suggested by Potter et al. (2005) for similar laminae. The chaotic textured muddy sandstones beds have been formed by multiple events of debrites. Early diagenetic formation of pyrite is favoured by anoxic conditions according to Potter et al. (2005), so the pyrite is an indication of anoxic water conditions when deposition happened or soon after. Pyrite requires three components to form, organic carbon, iron, and sulphate. Sulphates are always abundant in marine setting, so the control on how much pyrite is produce is the amount of iron and carbon in the sediment (Potter et al., 2005). Siderite-rich black shale beds and concretions may have formed in early diagenetic processes under marine conditions, possibly related to degradation reactions of organic content as suggested by Mørk et al. (2002). The glauconite clasts and bioturbation in the lower part of the logged section in core 7230/05-U-02 indicate low sedimentation rates, as suggested by Potter et al. (2005) for glauconite rich sediments. The broken-up section of the core can be interpreted as slumps due to the disturbed and chaotic texture, but it is hard to tell whether the broken-up section is from slumping or from later disturbances when drilling the core, due to the similar textures between slumps and disturbed sections of the core. The darker colour in core 7230/05-U-02 could be due to higher content of organic material in the black shale in core 7230/05-U-02, or higher clay fractions than in core 6307/07-U-03A. The organic content can affect the colour of sediment according to Potter et al. (2005). The total organic carbon in core 6307/07-U-02 (~2 km distance from core 6307/07-U-03A) is between 3.9 and 4.3 wt% (Langrock et al.,

2003), and the total organic carbon of core 7230/05-U-02 is between 7 to 23 wt% (Bugge et al., 2002), supporting the organic control on the colouring of the black shale.

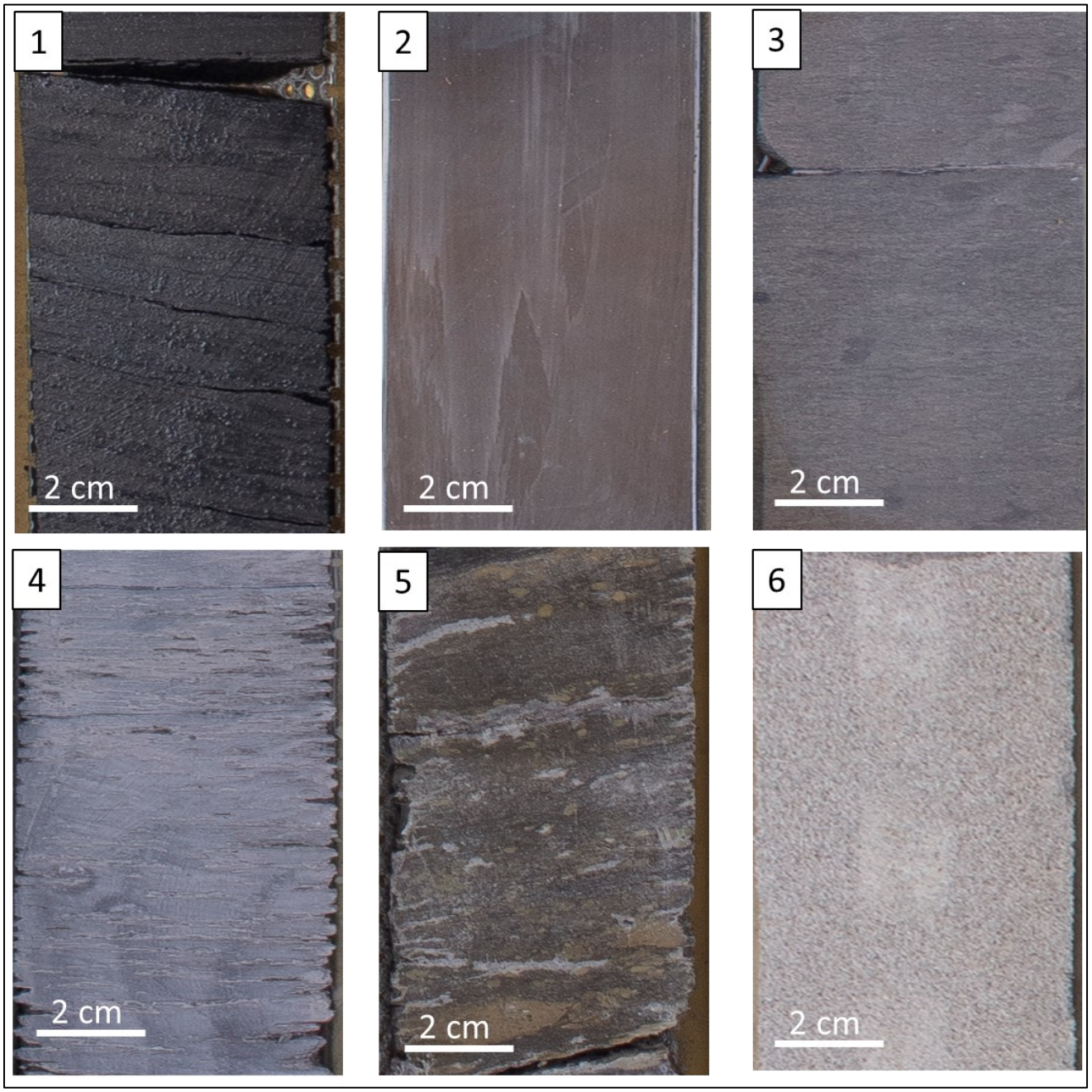

Figure 7. *Picture of the facies ; (1) laminated black shales, (2) iron-rich black shale, (3) muddy sandstone, (4) carbonate cemented shale, which is heavily varnished and demonstrates the effects the varnish can have on the core, (5) glauconite bedded shale, and (6) massive sandstone.*

Table 3. *Six facies with descriptions from the logging of core 6307/07-U-03A and 7230/05-U-02.*

Facies number	Name	Description
1	**Laminated black shale**	Shale with mainly clay sediments. Mostly black and grey small-scale horizontal planar laminae, reflecting differences in grain size, with grey laminae having more silt to fine sand. Calcified fossil fragments, pyrite and siderite concretions present in some black shale laminae.
2	**Iron-rich black shale**	Siderite and pyrite cemented black shale with mainly clay sediments. Concretions of siderite and pyrite up to pebble size. The thickness varies from mm to 20 cm beds. Red and brownish colour from oxidation of iron-rich minerals.
3	**Muddy sandstone**	Clay to fine sand size, grey and black colour reflecting the silt to fine sand and clay sediments, respectively. A chaotic texture of mainly silt and fine sand with mud clasts. High content of pyrite laminae and nodules, and some bioturbation. Only present in the upper part of core 6307/07-U-03A.
4	**Carbonate cemented shale**	Carbonate cemented shale bed with wavy ripple cross-lamination. Mainly clay sediments. Only present at ~42.5 m in core 6307/07-U-03A.
5	**Glauconite bedded shale**	Shale bed with a thickness of 10 cm containing glauconitised clasts of up to 2 cm. Black to grey colour. Glauconite clasts of beige colour from sand to pebble size. Some bioturbation. Only present in the lower 10 cm of core 7230/05-U-02.
6	**Massive sandstone**	Massive sandstone of mainly fine to medium sand size. Abundant of quartz grains in the sandstone. Only present in the top of core 6307/07-U-03A.

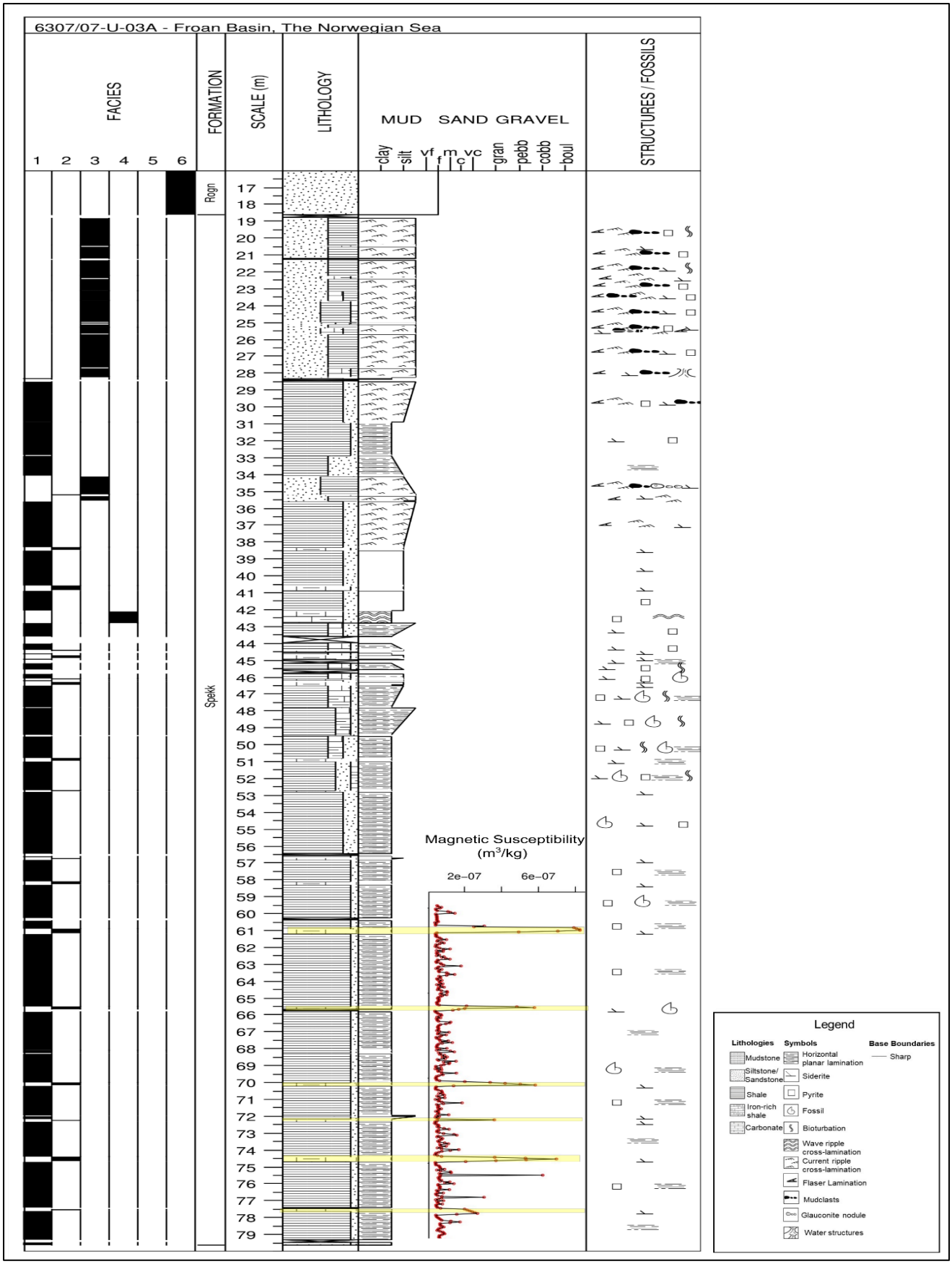

Figure 8. *Stratigraphy and magnetic susceptibility variations in core 6307/07-U-03A from the black shale section of the Spekk Formation in the Norwegian Sea. Linearly interpolated data in red.*

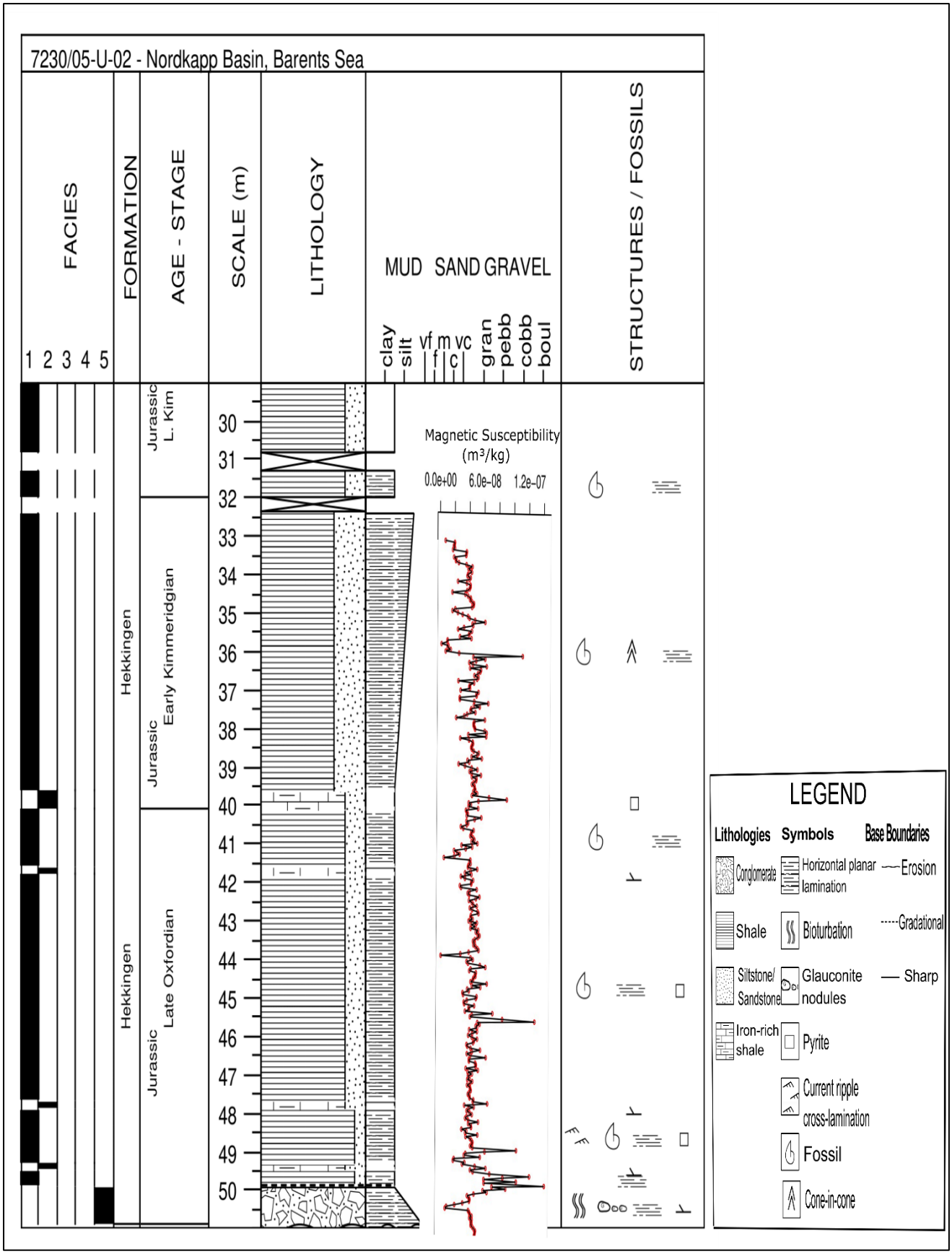

Figure 9. *Stratigraphy and magnetic susceptibility variations in core 7230/05-U-02 from the black shale section of the Hekkingen Formation in the Barents Sea. Linearly interpolated data in red. Stratigraphic age are from Wierzbowski and Smelror (1993).*

5.2. Magnetic Susceptibility and Spectral Analysis

Spekk Formation (Core 6307/07-U-03A)

The un-processed magnetic susceptibility measurements from the core in the Møre-Trøndelag area of the Norwegian Sea are shown in Figure 10. The measurements are taken from 79.65 m to 59.85 m depth in the core corresponding to an interval with laminated black shales and iron-rich black shale of mainly siderite nodules and cementation. The average value of the magnetic susceptibility is $9.5 \times 10^{-8}\ \mathrm{m^3 kg^{-1}}$. Most of the measured magnetic susceptibility values are between $4.0 - 12.0 \times 10^{-8}\ \mathrm{m^3 kg^{-1}}$ and will be defined as the background susceptibility. Six spikes in magnetic susceptibility values between $20 - 82 \times 10^{-8} \mathrm{m^3 kg^{-1}}$ are correlated with siderite cemented shale beds, suggesting a lithological control on magnetic susceptibility. The high magnetic susceptibility siderite cemented beds appear to have an even spacing, which indicates cyclicity. The data series with the siderite spikes is shown in Figure 11, and the processed data series without the siderite spikes is shown in Figure 13. From the data series without the siderite spikes, smaller cycles on a cm-scale are visible.

The un-processed magnetic susceptibility data series shows seven significant spectral peaks with a harmonic confidence limit criterion of 90 % or higher present in the MTM power spectrum (Figure 12). The description of the significant spectral peaks can be found in Table 4. The result reveal cycles with the ratio of period 1.12 m and 0.45 similar to the ratio of the short eccentricity cycle (95 ka) and the obliquity cycle (38 ka).

The processed magnetic susceptibility data series shows twelve significant spectral peaks with a harmonic confidence limit criterion of 90 % or higher present in the MTM power spectrum (Figure 14). The description of the significant spectral peaks can be found in Table 5. The power spectral reveal cycles with a ratio of the period 5.5 m, 0.32 m, and 0.15 m is similar to the ratio of the long eccentricity cycle (405 ka), the obliquity cycle (38 ka), and the precession cycle (~18.2 ka). The reason high-power peaks like the peak ~0.3 cycles per metre are not identified as significant, is that the harmonic f-test confidence level falls below the 90 % threshold. The high-power peak of ~0.3 cycles per metre has a harmonic confidence level of only 17 %, well below the 90 % confidence threshold for identifying statistically significant peaks.

An evolutionary spectrogram analysis was performed on the data series without the siderite beds (Figure 15). The spectrogram shows the dominant frequencies in the power spectrum through the section. The low frequency peaks under 1.0 cycles per metre (peaks nr. 1 and 2) have relatively high power throughout the whole section. There are relatively low power frequencies around 1.0 cycles per metre between 72 m and 66 m in the section. The low power area is the reason there are no significant spectral peaks around 1.0 cycles per metre in the core. High power areas throughout the section around 2.0 cycles per metre (peaks nr. 3 and 4), with relatively

higher power in the lower parts of the section from 70 m than in the upper section. Peaks around 3.0 cycles per metre (peaks nr. 5, 6, and 7) have a higher power in the upper part of the section down to 70 m than in the lower part. Peak between 4.5 and 5 cycles per metre (peaks. nr 8 and 9) have a relatively high power only in the upper 2.0 m of the section between 76 m and 74 m. The peaks around 6.0 to 6.5 cycles per metre (peaks nr. 10, 11, and 12) have a relatively high power in the middle part of the section between 70 m and 65 m. The dominant frequencies lower than 2.0 cycles per metre do not vary significantly in power, which indicates a stable sedimentation rate. However, the dominant frequencies higher than 2.0 cycles per metre vary, with a higher power in the upper parts of the section. This means that the sedimentation rates in the section are not stable.

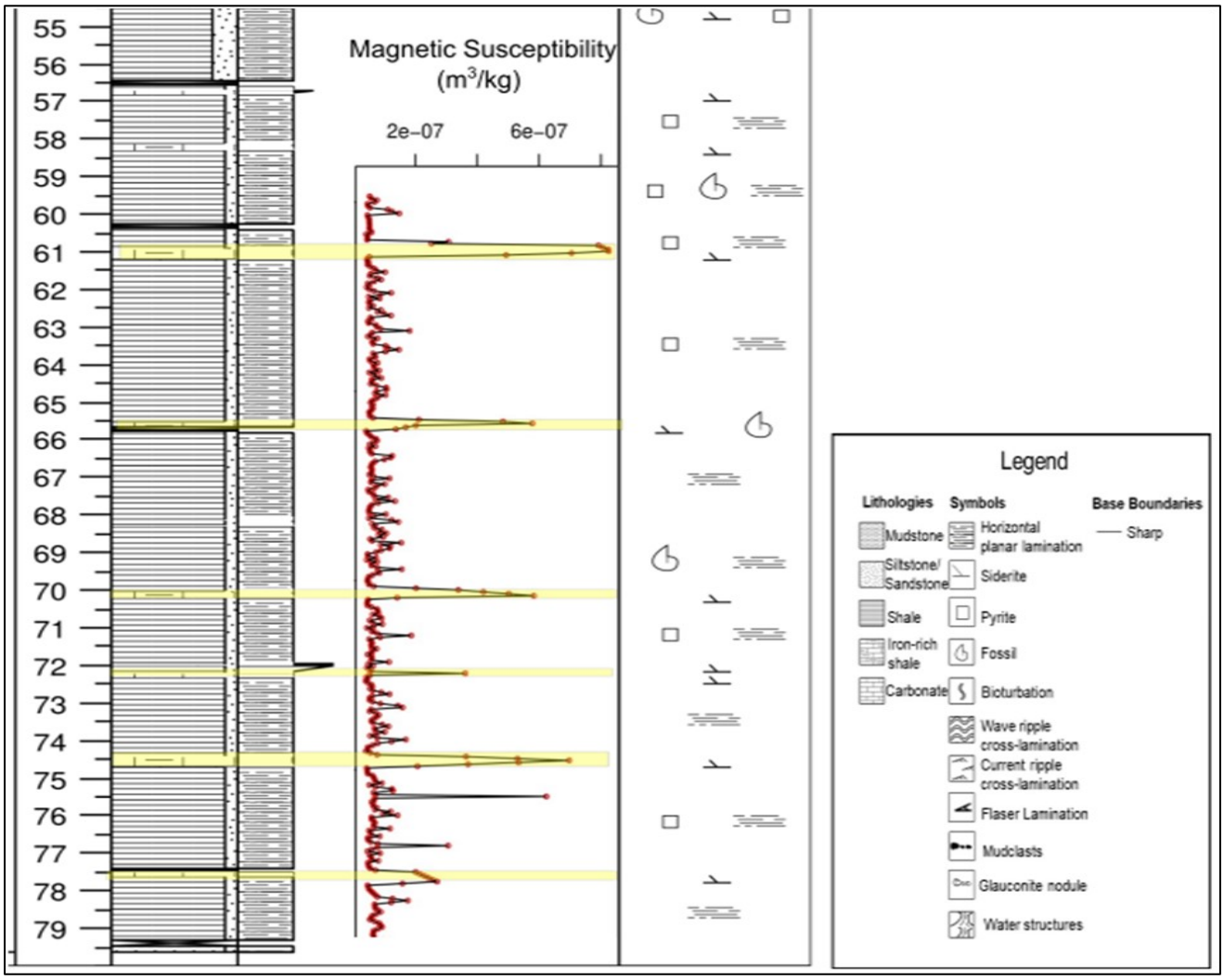

Figure 10. *Stratigraphy and magnetic susceptibility variations in core 6307/07-U-03A from the black shale section of the Spekk Formation in the Norwegian Sea. Linearly interpolated data in red. Zoomed in version of the log in Figure 8.*

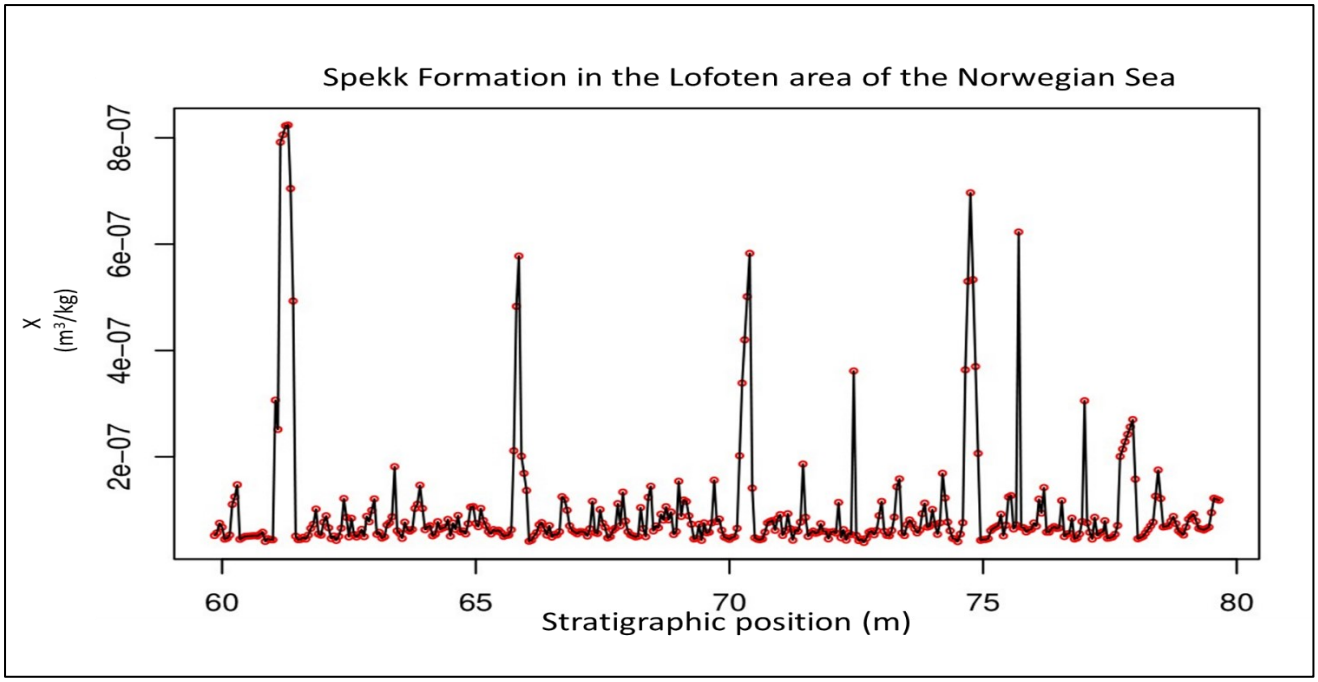

Figure 11. Magnetic susceptibility measurements from a 20 m section in core *6307/07-U-03A* from the black shales of the Spekk Formation in the Møre-Trøndelag area of the Norwegian Sea. The high susceptibility siderite beds are included.

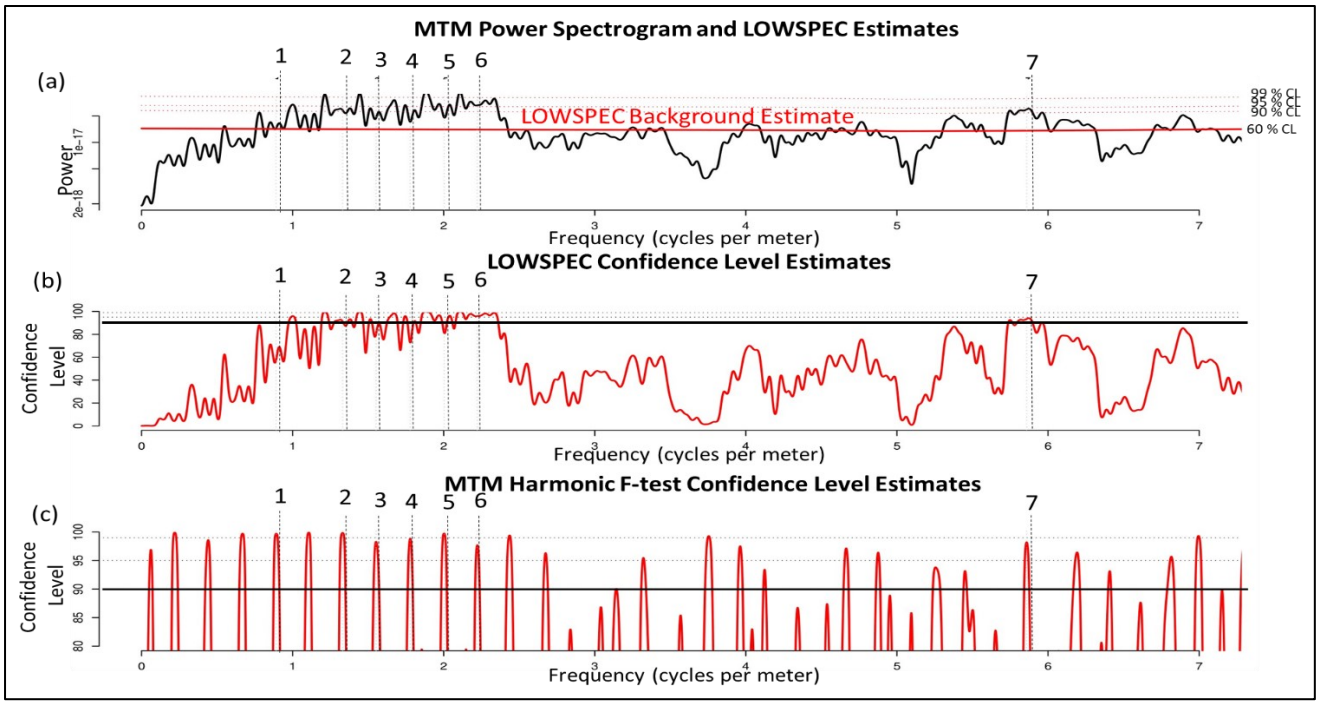

Figure 12. *MTM power spectrum for the magnetic susceptibility measurements in core 6307/07-U-03A from the black shales of the Spekk Formation in the Møre-Trøndelag area of the Norwegian Sea with the siderite beds included. (a) The MTM power spectrum identified seven significant peaks up to 7.0 cycles per metre. The 99%, 95%, and 90 % confidence levels are indicated on the spectrogram, and the 60 % LOWSPEC background estimate is indicated by the red line. The criteria for identification of significant spectral peaks are the (b) LOWSPEC confidence level set to 90 % indicated by the black line, and the (c) harmonic f-test confidence level set to 90 % indicated by the black line.*

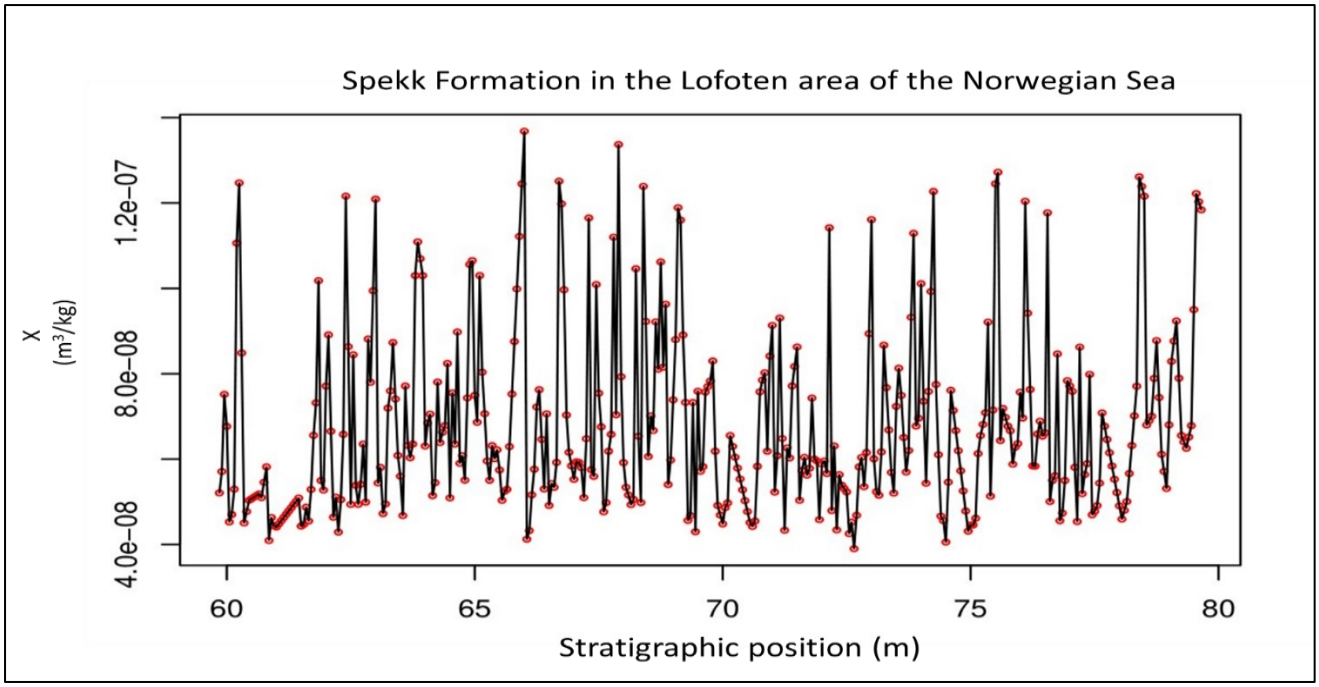

Figure 13. *Magnetic susceptibility measurements from a 20 m section in core 6307/07-U-03A from the black shales of the Spekk Formation in the Møre-Trøndelag area of the Norwegian Sea. Thirty-six data points have been removed because of high magnetic susceptibility values. Red dots are interpolated datapoints.*

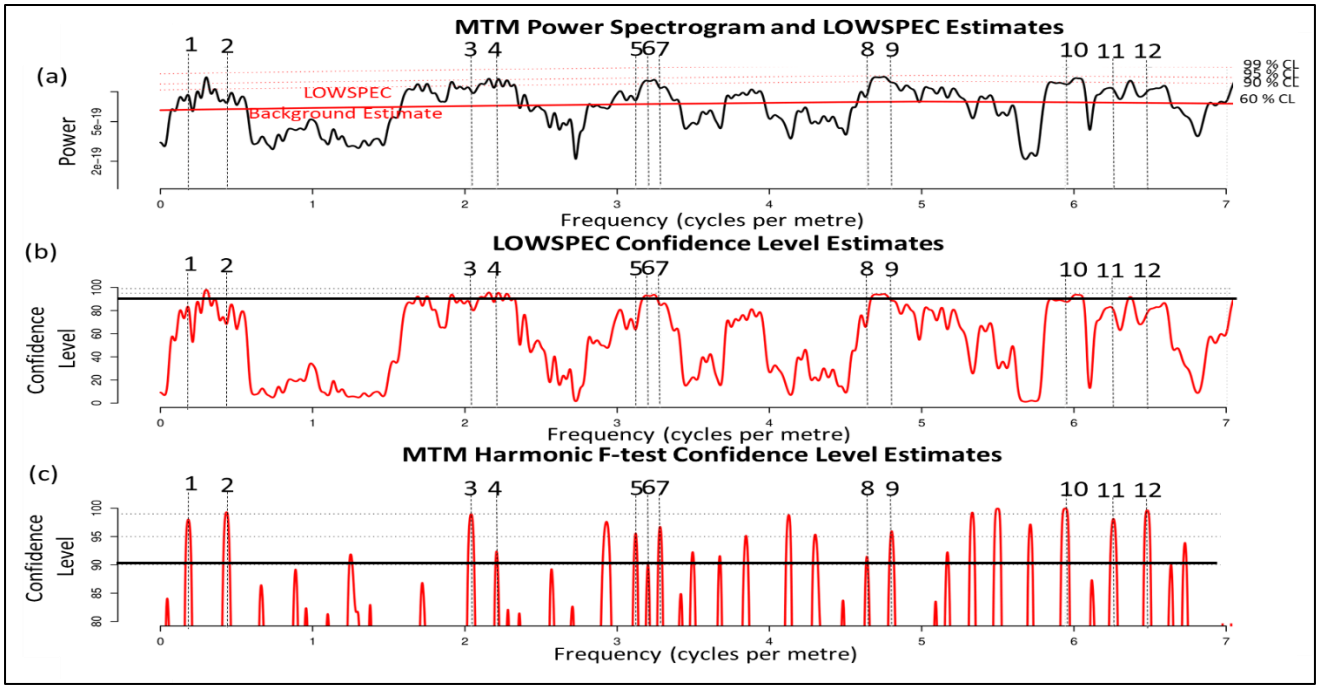

Figure 14. *MTM power spectrum for the magnetic susceptibility measurements in core 6307/07-U-03A from the black shales of the Spekk Formation in the Møre-Trøndelag area of the Norwegian Sea with the siderite beds removed. (a) The MTM power spectrum identified twelve significant peaks up to 7.0 cycles per metre. The 99%, 95%, and 90 % confidence levels are indicated on the spectrogram, and the 60 % LOWSPEC background estimate is indicated by the red line. The criteria for identification of significant spectral peaks are the (b) LOWSPEC confidence level set to 90 % indicated by the black line, and the (c) harmonic f-test confidence level set to 90 % indicated by the black line.*

Table 4. *Spectral peaks in core 6307/07-U-03A of the Spekk Formation from the Froan Basin in the Norwegian Sea with the siderite beds included. CL = confidence limit. Period A is calculated with a sedimentation rate of 1.16 cm/ka (Figure 16), and Period B is calculated with a sedimentation rate of 0.82 cm/ka taken from Mutterlose et al. (2003). The times marked in bold are within the uncertainty range of the Milankovitch periodicity in Table 1.*

Peak number	Frequency (cycles per metre)	Period (m)	Harmonic CL (%)	LOWSPEC CL (%)	Period A (ka)	Period B (ka)
1	0.892	1.121	99.7	58.4	96.6*	136.6
2	1.331	0.751	99.8	91.4	64.8	91.6
3	1.553	0.644	98.3	80.6	55.6	78.6
4	1.779	0.562	98.8	72.9	48.5	68.6
5	2.003	0.499	99.8	81.5	43	60.9
6	2.223	0.450	97.7	95.9	**38.8**	54.9
7	5.858	0.171	98.2	93.5	14.7	20.8

** The period of 96.6 ka has a 1.7 % deviation from the target eccentricity cycle (95 ka) in Table 1.*

Table 5. *Spectral peaks in core 6307/07-U-03A of the Spekk Formation from the Froan Basin in the Norwegian Sea without the siderite beds.CL = confidence limit. Period A is calculated with a sedimentation rate of 1.28 cm/ka (Figure 16), and Period B is calculated with a sedimentation rate of 0.82 cm/ka taken from Mutterlose et al. (2003). The times marked in bold are within the uncertainty range of the Milankovitch periodicity in Table 1.*

Peak number	Frequency (cycles per metre)	Period (m)	Harmonic CL (%)	LOWSPEC CL (%)	Period A (ka)	Period B (ka)
1	0.183	5.455	98.1	83.1	426.2*	665.3
2	0.435	2.301	99.4	68.4	252.8	394.6*
3	2.041	0.490	99.0	83.1	**38.3**	59.7
4	2.208	0.453	92.1	93.2	35.4	55.2
5	3.122	0.320	95.5	63.7	**25.0**	**39.0**
6	3.202	0.312	90.4	92.9	**24.4**	**38.1**
7	3.282	0.305	96.5	84.8	**23.8**	**37.2**
8	4.640	0.216	92.3	69.5	16.8	26.3
9	4.804	0.208	95.8	88.7	16.2	25.4
10	5.943	0.168	99.9	87.7	13.1	20.5
11	6.259	0.160	98.2	80.6	12.5	19.5
12	6.482	0.154	99.7	78.0	12.1	**18.8**

**The period of 426.2 ka has a 5.2 % deviation, and the period of 394.6 ka has a 2.6 % deviation from the eccentricity period (405 ka) in Table 1.*

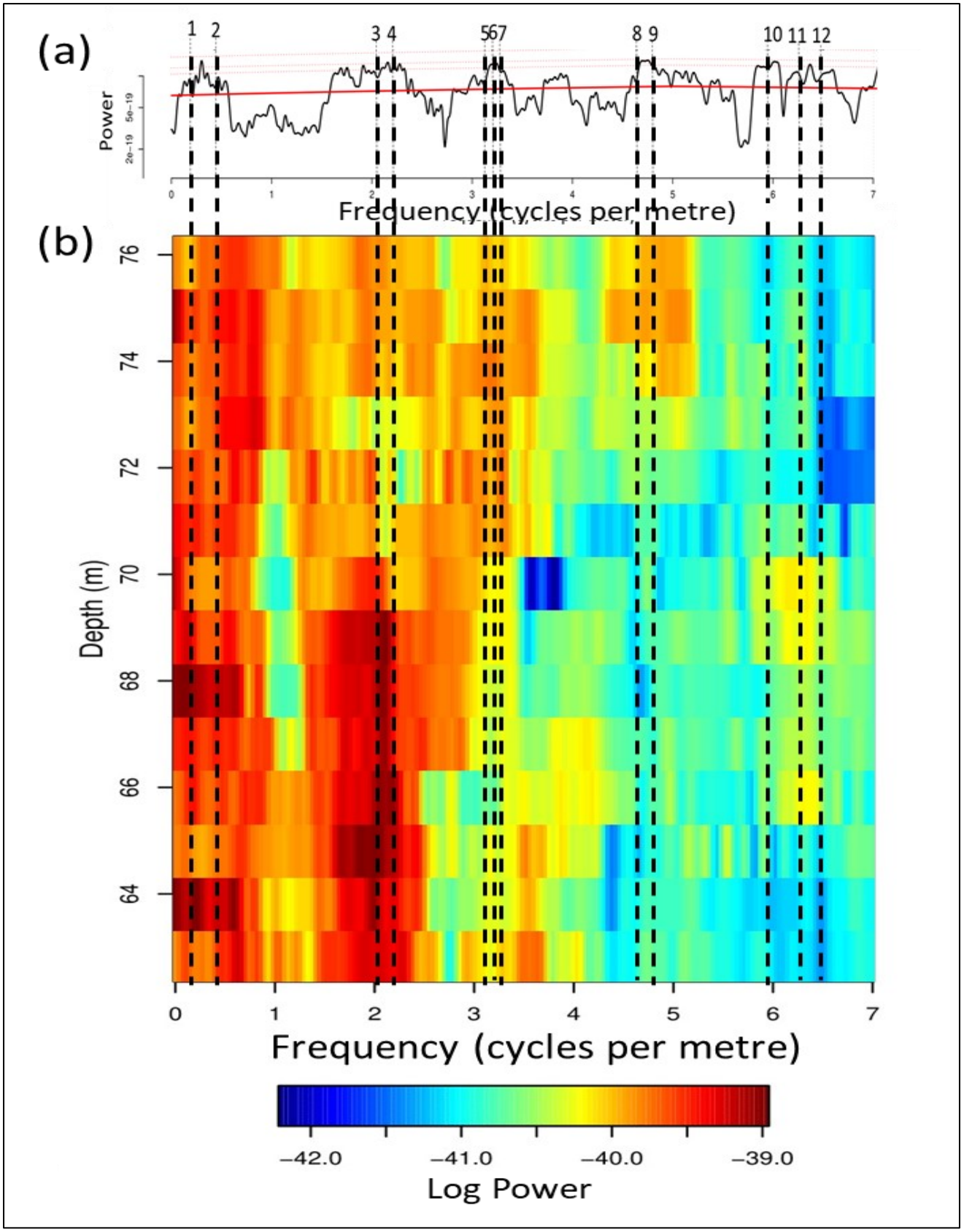

Figure 15. *Power evolutionary spectrogram from core 6307/07-U-03A calculated by Astrochron. (a) The MTM power spectrum from Figure 14 compared with (b) the evolutionary spectrogram calculated with a window of 6 m and a step of 1 m. The power of the frequencies varies within the section.*

Table 5 shows the time duration of the periods from the significant peaks calculated with the sedimentation rate from the TimeOpt method (Period A), and the sedimentation rate from Mutterlose et al. (2003) (Period B). The periods in Table 4 are from the data series with the siderite beds, and the periods in Table 5 are from the data series without the siderite beds. The TimeOpt analysis of the data series identified an optimized sedimentation rate of 1.16 cm/ka for the section with the siderite beds (Figure 16 a), and 1.28 cm/ka for the section without the siderite beds (Figure 16 b). The sedimentation rate from the TimeOpt method yields seven periods that correlate to Milankovitch cycles, with five periods achieving the uncertainty range in Table 1. The period of 426.2 ka (Table 5) correspond to the 405 ka long eccentricity cycle. However, the 21 ka difference between the calculated and target period (5.2 %) can be judged to be too far away to be the eccentricity cycle. The period of 96.6 ka (Table 4) corresponds to the short eccentricity cycle of 95 ka. The period of 38. 8 ka (Table 4) and 38.3 ka (Table 5) is within the uncertainty range of the main obliquity cycle of 38.0 ka. The periods of 25.0 ka, 24.4 ka, and 23.8 ka (Table 5) all fall within the uncertainty range of the Earth axis precession period of 24.48 ka.

In order to analyse the variation in sedimentation rates found in the evolutionary spectrogram analysis (Figure 15), a template was included in the TimeOpt method. The template takes into consideration different sedimentation patters. For the section with the siderite beds the average sedimentation rate is 1.19 cm/ka, with variations from 1.15 cm/ka to 1.64 cm/ka, yielding a total duration of 1.67 Ma for the 20 m section (Figure 17 a). The high sedimentation rates are correlated with the siderite beds. For the section with the siderite beds removed, the average sedimentation rate is 1.29 cm/ka, with a variation from 1.26 cm/ka to 1.35 cm/ka, yielding a total duration of 1.54 Ma for the section (Figure 17 b). The smaller duration (~130 ka) in the section with the siderite beds removed is expected. The difference between the average sedimentation rates calculated by the TimeOpt method with a constant sedimentation rate (Figure 16), and with a varying sedimentation rate (Figure 17) is negligible.

Mutterlose et al. (2003) estimated a sedimentation rate of 0.82 cm/ka in core 6307/07-U-02. Assuming the sedimentation rate is similar in core 6307/07-U-03A results in seven periods that can correspond to Milankovitch cycles, with four periods within the uncertainty range in Table 1. The period of 394.6 ka (Table 5) corresponds to the 405 ka long eccentricity cycle, however, the deviation from the target period (2.7 %) is larger than the uncertainty of the eccentricity cycle. The period of 91.6 ka (Table 4) corresponds to the 95 ka short eccentricity cycle (Table 1). The periods of 39.0 ka, 38.1 ka, and 37.2 ka (Table 5) are within the uncertainty range of the 38 ka obliquity cycle (Table 1). The period of 20.8 ka corresponds to the 21.56 ka precession cycle (Table 1). And the period of 18.8 ka (Table 5) is within the uncertainty range of the 18.4 ka precession cycle (Table 1).

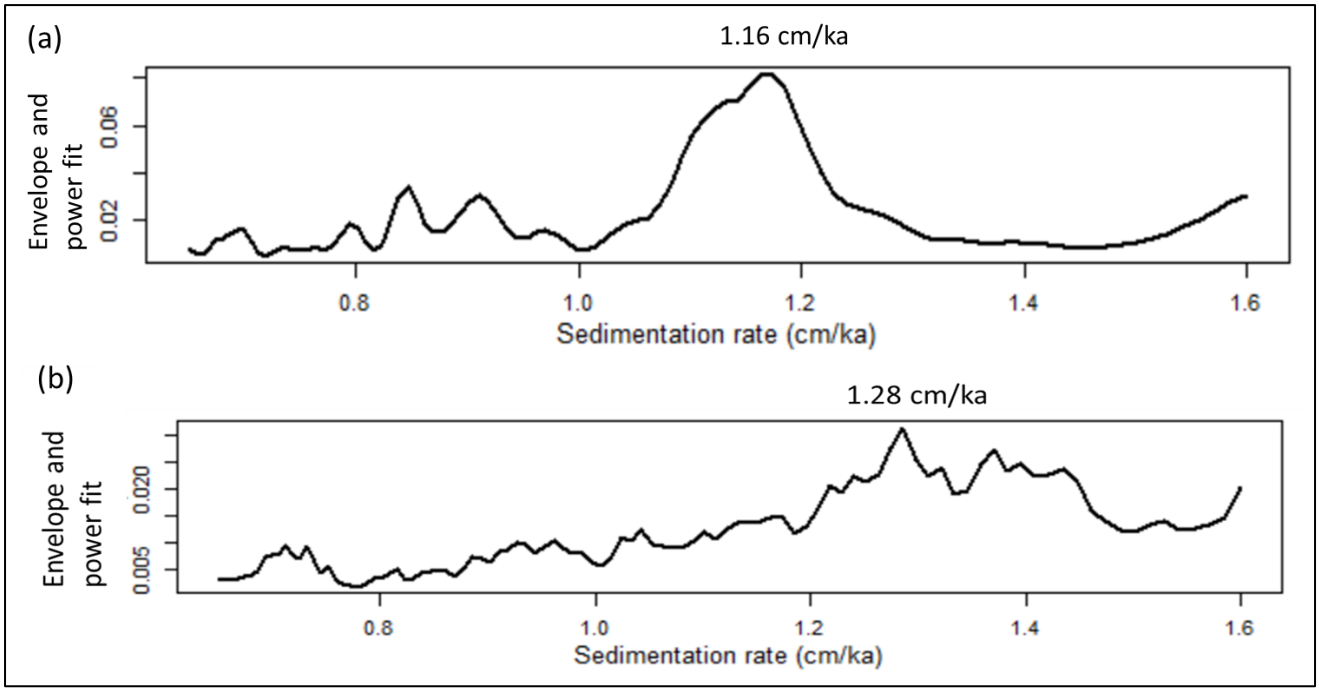

Figure 16. *TimeOpt analysis of the average sedimentation rate in core 6307/07-U-03A of the black shales of the Spekk Formation calculated by astrochron. (a) With the siderite beds the most optimal fit for the sedimentation rate is 1.16 cm/ka, and (b) with the siderite beds removed the most optimal fit for the sedimentation rate is 1.28 cm/ka.*

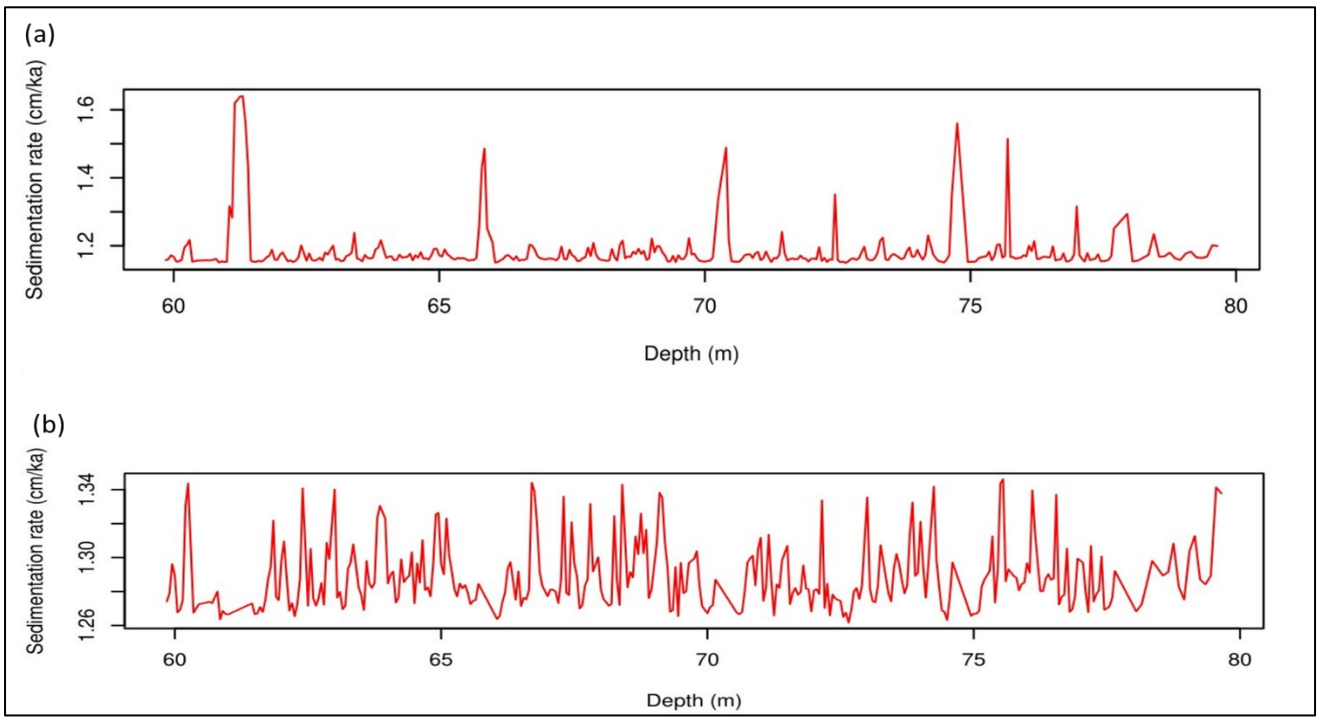

Figure 17. *TimeOpt analysis of varying sedimentation rates in core 6307/07-U-03A of the Spekk Formation calculated by astrochron, with a template taking into consideration different sedimentation models. (a) Varying sedimentation rates throughout the section with the siderite beds included. (b) Varying sedimentation rates throughout the section without the siderite beds.*

Hekkingen Formation (Core 7230/05-U-02)

The un-processed bulk magnetic susceptibility measurements from the Møre-Trøndelag area of the Norwegian Sea are shown in Figure 9. The measurements are taken from 33.15 m to 52.05 m depth in the core, corresponding to the whole black shales section in the core. The average magnetic susceptibility is $4.3 \times 10^{-8}\ \mathrm{m^3 kg^{-1}}$, with most of the magnetic susceptibility measurements between $3.0 - 6.0 \times 10^{-8}\ \mathrm{m^3 kg^{-1}}$, slightly lower than the most susceptibility values in core 6307/087-U-03A. Some of the pyrite rich beds have little to no control on the magnetic values. Higher magnetic susceptibility values than the average susceptibility can be found at the bottom of the section above the erosional contact between 49 m and 50 m. Siderite and pyrite laminae and nodules can be found between the 49 m and 50 m depths, so the siderite and pyrite are the likely source of the higher values. The magnetic susceptibility values are higher at ~45.5 m, however, this area has no visible iron-rich black shales facies. There is also a spike in magnetic susceptibility values at ~40 m correlated with an iron-rich shale bed. The magnetic values are slightly lower at the top of the core from ~36 m. This can indicate a lithological control with a higher content of silt and fine sand towards the top of the core generating lower magnetic susceptibility values. The cone-in cone structure at ~36 m can be correlated with higher magnetic susceptibility values. The data series were linearly interpolated, as shown in Figure 18, and a section of the data series from 33.15 m to 40 m corresponding to the black shale with a higher fraction of silt and sand is shown in Figure 20. Small cycles on a cm scale are present in the recorded magnetic susceptibility series.

The magnetic susceptibility data series shows 12 significant spectral peaks with a harmonic confidence limit criterion of 90 % or higher present in the MTM power spectrum (Figure 19). The description of the significant spectral peaks can be found in Table 6. An MTM power spectrum was also constructed for the upper part of the section from 33.15 m to 40.0 m. This interval has more silt and fine sand than the rest of the section, and has three significant spectral peaks (Figure 21). A description of the significant peaks can be found in Table 7.

The result of the power spectrum reveals cycles with a ratio of the periods of 1.1 m, 0.45 m, and the periods in the 0.2 m range have a similar ratio as the short eccentricity cycle (95 ka), the obliquity cycle (38 ka), and the precession cycles (~18.2 ka).

An evolutionary spectrogram analysis was performed on the data series (Figure 22). The spectrogram shows the power of the frequencies in the spectrum through the section. All significant peaks are indicated in the spectrogram. The power is relatively high in the lower frequencies up to 1.0 cycle per metre containing peaks nr. 1-4 in the upper part of the section from 48.8 m to 47.9 m. The power is lower from 47.9 m to 44.6 m, before the power is higher in the low frequencies again from 44.6 m to 36 m. From ~44.0 m the dominant frequencies go up gradually from 1.5 to 2.5 cycles per metre at the bottom of the spectrogram. The power is relatively high in the bottom parts around 2.0 cycles per metre containing peak nr. 5. The frequencies between 4.0 to 5.0 cycles per metre containing peaks nr. 6-8 have lower power than the peak at the lower frequencies. The highest power

can be found in the top 1.0 m of the spectrum, and the bottom 4 m between 40 m and 36m. The highest power is located around 5.0 cycles per metre in the top and around 4.0 cycles per metre in the bottom. Between 5 and 8 cycles per metre the power is low compared to the lower frequencies. Peak nr. 9-11 located at 6.0 cycles per metre has the highest power in the top 2.0 m and the bottom 4.0 m of the spectrogram. The frequencies between 8 and 9 cycles per metre have a low power compared to the lower frequencies. Peak nr. 12 are located between 8 and 9 cycles per metre, and have the highest power at the bottom 5.5 m between 41.5 m and 36 m. The power of the frequencies changes from ~ 40.0 m; this coincides with more silty and sandy shale in the upper part of the section (Figure 9). The change in the dominant frequencies throughout the section indicate a variation in the sedimentation rate.

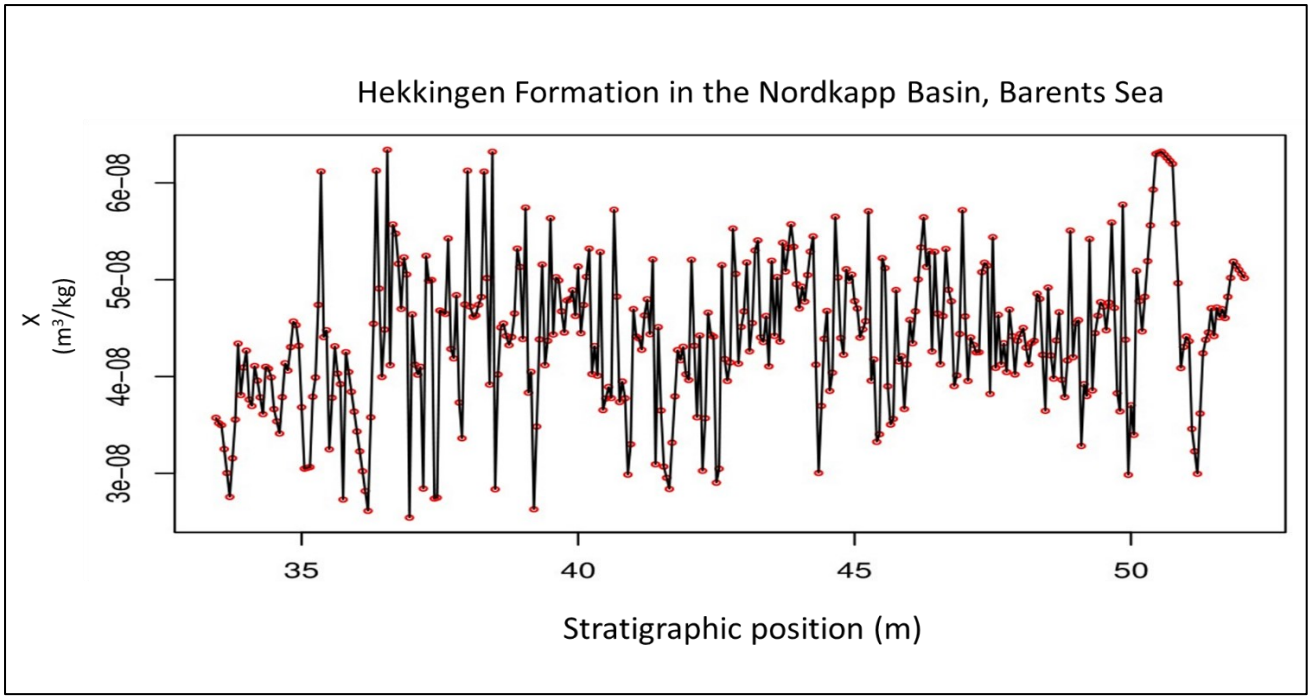

***Figure 18**. Data series of magnetic susceptibility measurements from a 20 m section in core 7230/05-U-02 from the black shales of the Hekkingen Formation in the Nordkapp Basin of the Barents Sea. Red dots are interpolated datapoints.*

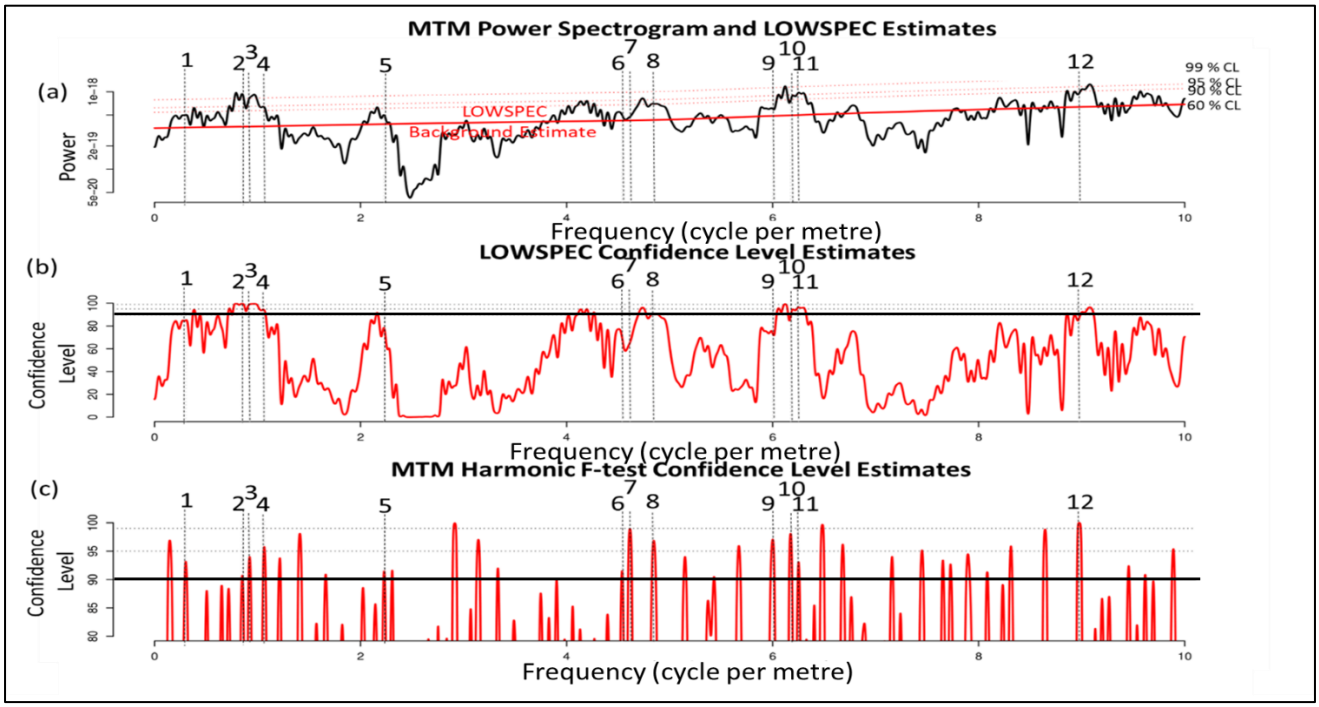

***Figure 19.** MTM power spectrum for the magnetic susceptibility measurements in core 7230/05-U-02 from the black shales of the Hekkingen Formation in the Barents Sea. (a) The MTM power spectrum identified twelve significant peaks up to 10.0 cycles per metre. The 99%, 95%, and 90 % confidence levels are indicated on the spectrogram, and the 60 % LOWSPEC background estimate is indicated by the red line. The criteria for identification of significant spectral peaks are the (b) LOWSPEC confidence level set to 90 % indicated with the black line, and the (c) harmonic f-test confidence level set to 90 % indicated by the black line.*

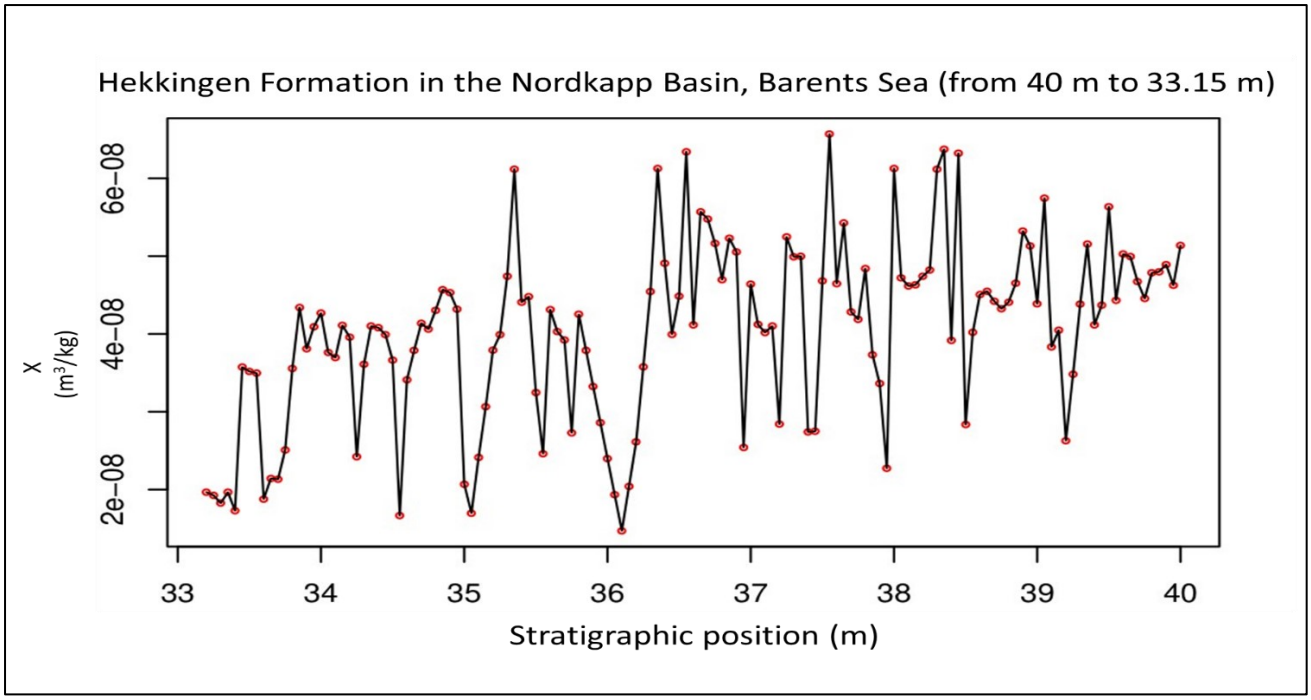

Figure 20. *Data series of magnetic susceptibility measurements from a 7 m section in core 7230/05-U-02 from 33.15 m to 40 m from the black shales of the Hekkingen Formation in Nordkapp Basin of the Barents Sea.The interval has a higher fraction of silt and sand grains than the rest of the core.*

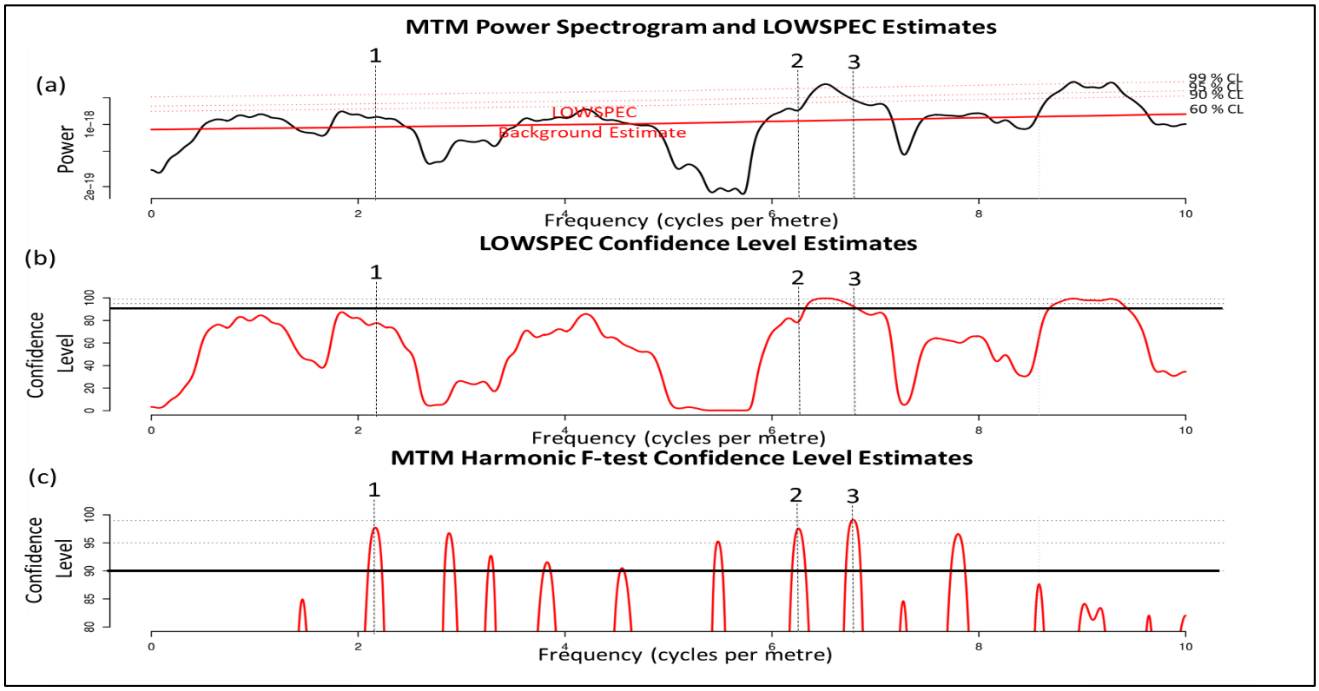

Figure 21. *MTM power spectrum for the magnetic susceptibility measurements in core 7230/05-U-02 from 33.15 m to 40 m in the black shales of the Hekkingen Formation in the Barents Sea. (a) The MTM power spectrum identified three significant peaks up to 10.0 cycles per metre. The 99%, 95%, and 90 % confidence levels are indicated on the spectrogram, and the 60 % LOWSPEC background estimate is indicated by the red line. The criteria for identification of significant spectral peaks are the (b) LOWSPEC confidence level set to 90 % indicated by the black line, and the (c) harmonic f-test confidence level set to 90 % indicated by the black line.*

Table 6. *Spectral peaks in core 7230/05-U-02 from the Hekkingen Formation of the Nordkapp Basin in the Barents Sea. CL = confidence limit. Period A is calculated with a sedimentation rate of 1.147 cm/ka (Figure 23), and Period B is calculated with a sedimentation rate of 0.5 cm/ka taken from Georgiev et al. (2017). The times marked in bold are within the uncertainty range of the Milankovitch periodicity in Table 1.*

Peak number	Frequency (cycles per metre)	Period (m)	Harmonic CL (%)	LOWSPEC CL (%)	Period A (ka)	Period B (ka)
1	0.303	3.299	93.2	85.0	289.4	659.9
2	0.852	1.174	90.7	99.7	103.0	234.9
3	0.924	1.083	94.0	99.1	**95.0**	216.5
4	1.066	0.938	95.7	94.2	82.3	187.7
5	2.229	0.449	91.5	78.0	**39.4**	89.7
6	4.539	0.220	91.5	69.9	19.3	44.1
7	4.615	0.217	98.9	65.5	19.0	43.3
8	4.846	0.206	96.9	90.7	**18.1**	41.2
9	6.001	0.167	97.1	73.5	14.6	33.3
10	6.174	0.162	98.1	88.3	14.2	32.4
11	6.252	0.160	93.1	96.5	14.0	32.0
12	8.976	0.111	99.9	87.0	9.8	**22.3**

Table 7. *Spectral peaks in core 7230/05-U-02 from the Hekkingen Formation of the Nordkapp Basin in the Barents Sea from 33.15 m to 40 m in the core. CL = confidence limit. Period A is calculated with a sedimentation rate of 1.147 cm/ka (Figure 23). and Period B is calculated with a sedimentation rate of 0.5 cm/ka taken from Georgiev et al. (2017).*

Peak number	Frequency (cycles per metre)	Period (m)	Harmonic CL (%)	LOWSPEC CL (%)	Period A (ka)	Period B (ka)
1*	2.166	0.462	97.7	77.6	40.5	92.3
2	6.257	0.160	97.6	78.9	14.0	32.0
3	6.786	0.147	99.1	92.5	12.9	29.5

** The significant level had to be lowered to 87 % for the peak to be significant.*

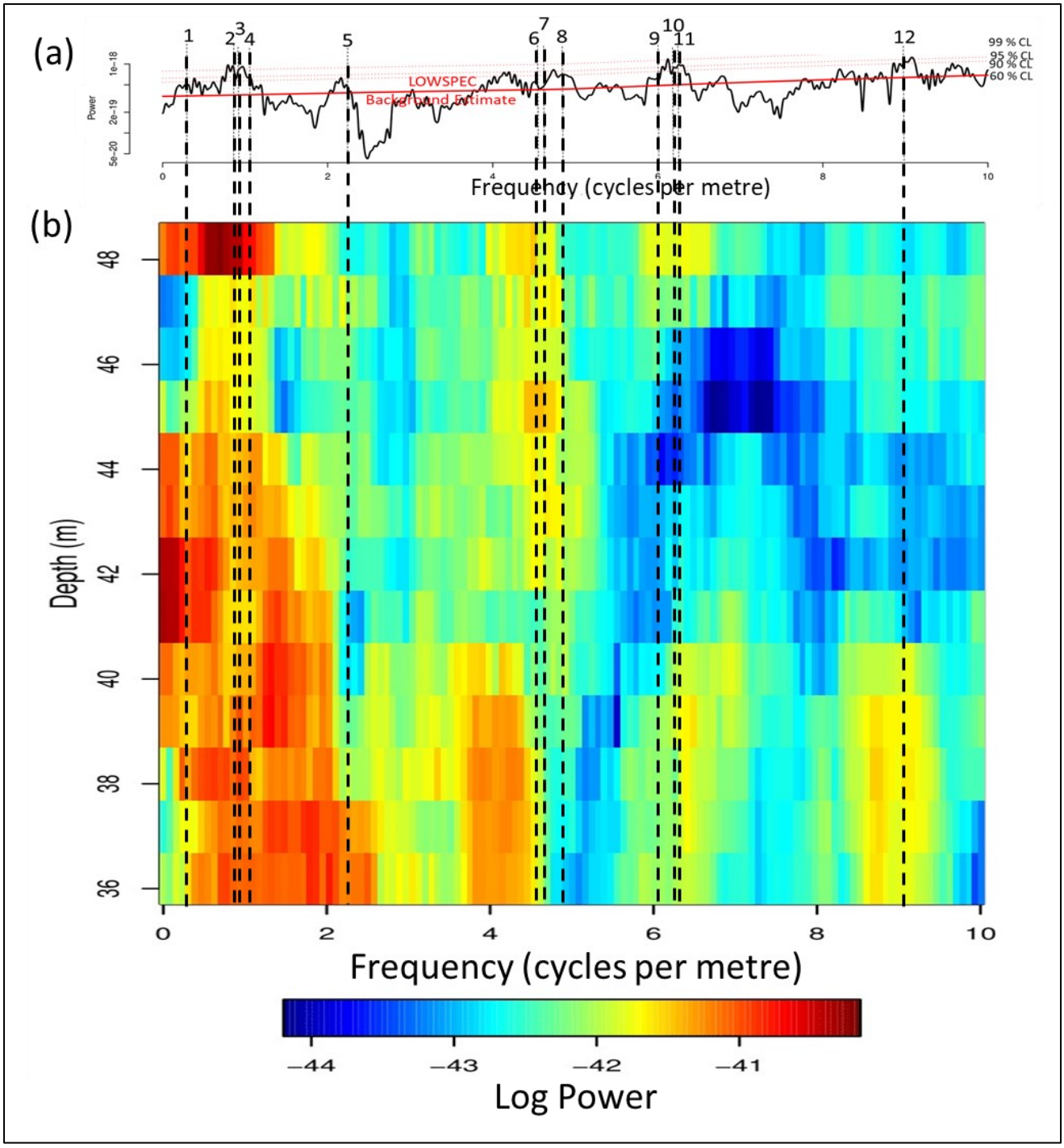

Figure 22. *Power evolutionary spectrogram in core 7230/05-U-02 calculated by Astrochron. (a) The MTM power spectrum from Figure 19 compared with (b) the evolutionary spectrogram calculated with a window of 6 m and a step of 1 m. The dominant frequencies varies within the section, indicating a variation in sedimentation rates.*

The TimeOpt analysis of the data series identified an optimized sedimentation rate of 1.14 cm/ka (Figure 23). The optimal sedimentation rate was similar for the whole section, and the 33.15 m to 40 m section. Table 6 and Table 7 show the time duration of the periods calculated with the sedimentation rate from the TimeOpt method (Period A), and the sedimentation rate taken from Georgiev et al. (2017) (Period B). The sedimentation rate from the TimeOpt method yields six periods that correlate to Milankovitch cycles, with four periods within the uncertainty range given in Table 1. The period of 120.4 ka (Table 6) corresponds to the 124 ka short eccentricity cycle, however, the period falls outside the uncertainty of the 124 ka period (2.8 % deviation from the 124 ka period). The period of 94.0 ka (Table 6) corresponds to the 95.0 ka short eccentricity cycle. The period of 40.1 (Table 7) corresponds to the 38 ka obliquity cycle, though the period is not within the 4.5 % uncertainty estimated in Table 1. The period of 21.5 ka (Table 6) corresponds to the 21.46 ka precession cycle, and the periods 18.9 ka and 18.2 ka (Table 6) correspond to the 18.43 ka and 18.29 ka precession cycles respectively.

In the analysis of the varying sedimentation rates, the TimeOpt template were used. The average sedimentation rate is 1.12 cm/ka, with variations from 0.84 cm/ka to 1.81 cm/ka, yielding a total duration of 1.68 Ma for the whole section (Figure 24). The difference between the average sedimentation rates calculated by the TimeOpt method with a constant sedimentation rate (Figure 23), and with a varying sedimentation rate (Figure 24) is negligible.

Georgiev et al. (2017) estimated a sedimentation rate of 0.5 cm/ka for the Hekkingen Formation in core 7230/05-U-02. Using this sedimentation rate results in five periods correlated to Milankovitch cycles. The period of 92.5 ka (Table 7) corresponds to the 95.0 ka short eccentricity cycle, though the period is not within the uncertainty. The period of 41.9 ka (Table 6) corresponds to the 38 ka obliquity cycle, though the period is not within the uncertainty of 4.5 % estimated in Table 1. The period of 24.2 ka (Table 6) corresponds to the 24.48 Earth axis precession cycle, and the periods of 22.9 ka and 22.3 ka (Table 6) correspond to the 22.65 ka precession cycles. Due to the sampling interval of 0.5 cm and a sedimentation rate of 0.5 cm/ka, the shortest period that could be found in the spectral analysis is the 20 ka period. This means that precession cycles ~18 ka will fall outside the spectrogram.

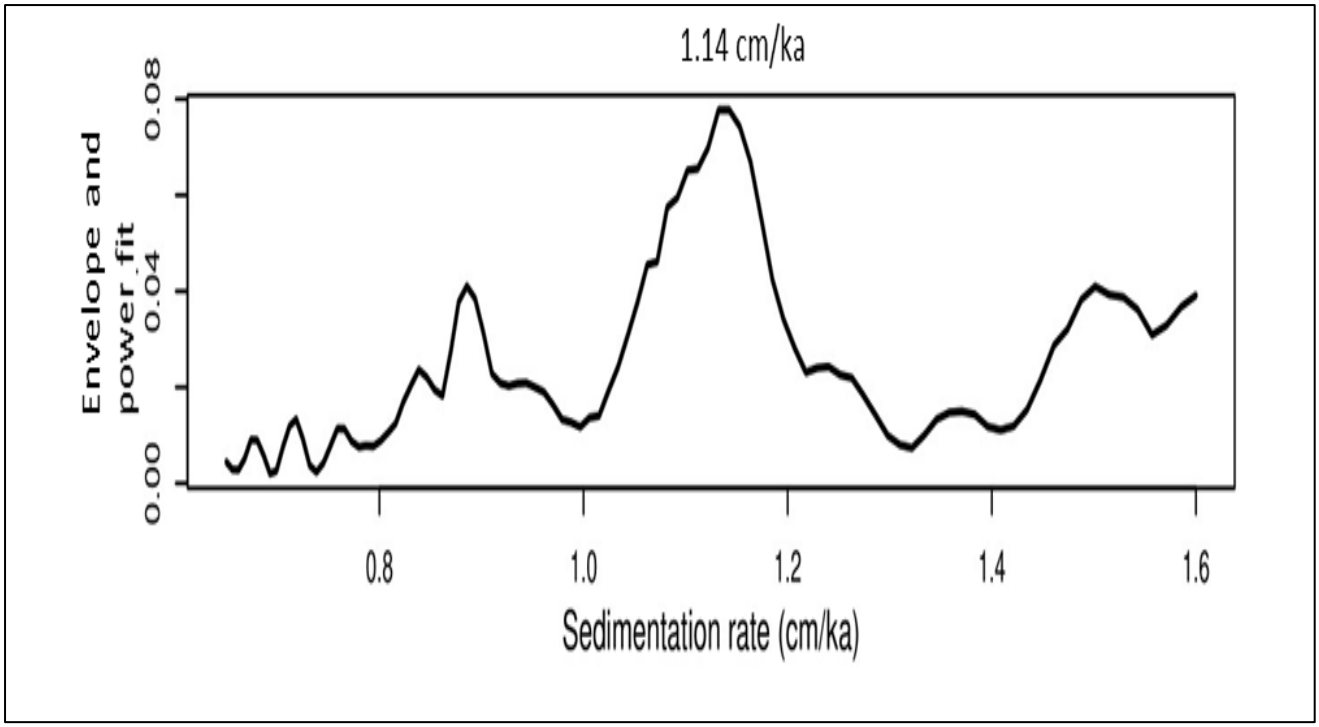

Figure 23. *TimeOpt analysis of the average sedimentation rate in core 7230/05-U-02 from the black shales of the Hekkingen Formation calculated by astrochron. The most optimal fit for the sedimentation rate is 1.14 cm/ka.*

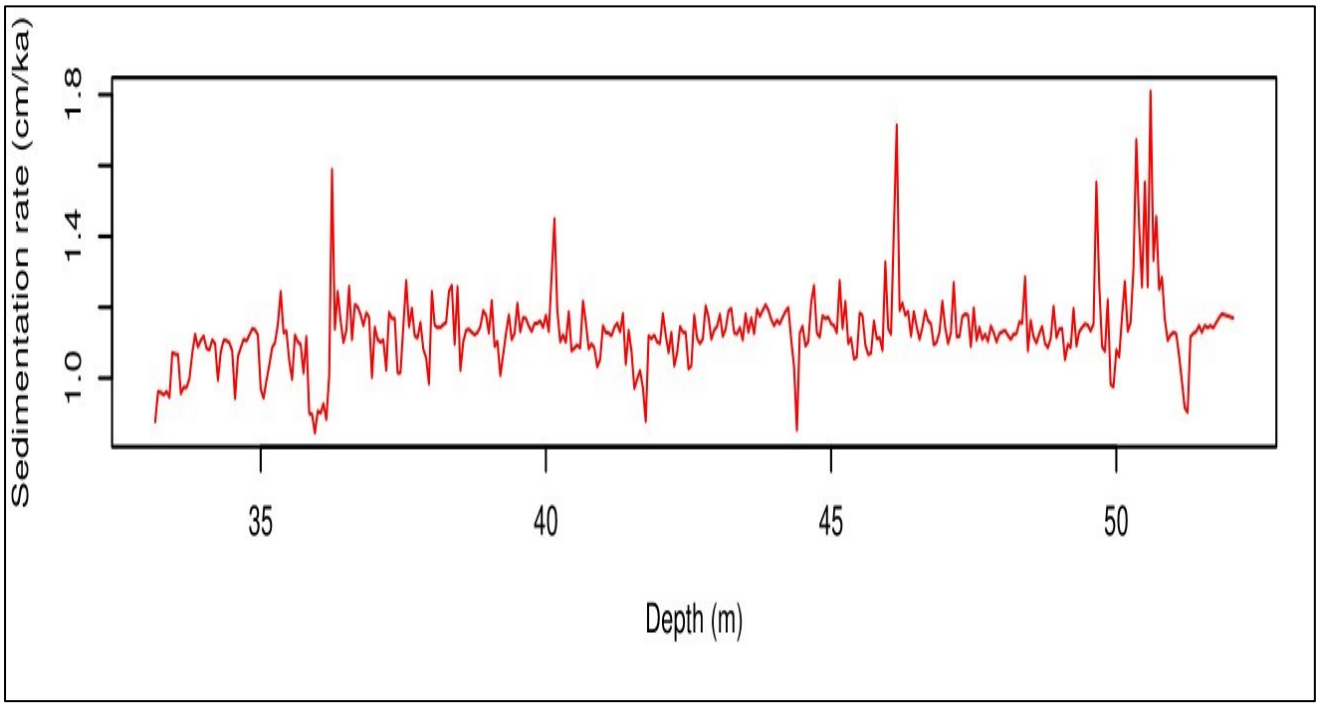

Figure 24. *TimeOpt analysis of the varying sedimentation rates in core 7230/05-U-02 from the Hekkingen Formation calculated by astrochron with a template taking into consideration different sedimentation models.*

6. Discussion

6.1. Uncertainties in the Method

The duration of the cycles indicated by the significant peaks in the spectrogram depends on the sedimentation rate of the black shales. Two sedimentation rates are used for each core to calculate the duration of the periods. Sedimentation rates were estimated by Mutterlose et al. (2003) for core 6307/07-U-02, and by Georgiev et al. (2017) for core 7230/05-U-02. Sedimentation rates are also calculated by an algorithm identifying the sedimentation rate that simultaneously optimizes eccentricity modulation within the precession cycles, and concentrates power at specified target periods. An assumption of the TimeOpt method is that the algorithm presupposes orbital cycles in the Milankovitch range. The two sedimentation rates that were used differ by a factor 2-3. In core 6307/07-U-03A the sedimentation rate of 0.82 cm/ka is used in the calculation of the periods were taken from core 6307/07-U-02.

The difference in the sedimentation rates between the estimated TimeOpt method and the sedimentation rate taken from Mutterlose et al. (2003) in core 6307/07-U-03A may stem from the fact that the sedimentation rate was taken from the neighbouring core (6307/07-U-02). This may cause the sedimentation rate to vary if the lateral conditions in the Basin are different between the cores, or the sedimentation rates may be calculated from another formation in the core than the black shale formation in core 6307/07-U-03A. In addition, according to the astronomically calculated sedimentation rates in Table 2, the lowest possible sedimentation rate recorded in type B cycles with the siderite concretions beds similar to that found in 6307/07-U-03A is 1.58 cm/ka. This means that the sedimentation rate of 1.16 cm/ka estimated for 6307/07-U-03A is 0.42 cm/ka away from the sedimentation rates estimates in similar siderite concretions beds. The difference in sedimentation rates between the estimates from the TimeOpt method and the sedimentation rate taken from Georgiev et al. (2017) in core 7230/05-U-02 is 0.64 cm/ka. However, Georgiev et al. (2017) estimated a sedimentation rate of 1.68 cm/ka for the Alge Member of Hekkingen Formation in the Troms III area, leading to a substantial range in the difference between the sedimentation rates in the Troms III area and in the Nordkapp Basin (236 % deviation). There are uncertainties in the thickness of the black shale formations in the Nordkapp Basin (Georgiev et al., 2017). The uncertainty in the thickness of the black shale formation will also lead to uncertainty in the estimated sedimentation rate. In conclusion the estimate from the TimeOpt method is within reasonable sedimentation rates expected in the black shales of the Spekk and Hekkingen Formation.

Uncertainties in the sedimentation rate arise from uncertainties in the depth control of the sampled rocks due to reshuffled core material. It is hard to quantify the uncertainty in the measured depth. However, most of the samples have been correlated to the display half of the core with high accuracy. Only a small section of the sampled half has reshuffling of core material (~5 %), and most of the reshuffled material was successfully correlated with the display core, which has fixed depth control. The correlation of siderite beds with the high

magnetic susceptibility values shows the depth control in Figure 10. The siderite beds are logged with established depth control from the presentation half of the cores. If the sampled depths for the susceptibility measurements had been wrong, the high magnetic susceptibility peaks would not be correlated with all the siderite beds, and the correlation between the siderite beds and the high magnetic susceptibility would be slightly shifted. There is no established method that is accepted as a standard when reporting uncertainties in a cyclostratigraphic study (Sinnesael et al., 2019). Another source of uncertainty is the processing of data, such as interpolation of gaps in the sequence, removal of outliers, and use of windows to mitigate edge effects. There is also uncertainty in the degree of compaction in the sediments so the decompaction factor is not known, this could possibly alter the sedimentation rates during deposition.

The Cyclostratigraphy Intercomparison Project (CIP) assessed the robustness of the method using artificial cyclostratigraphic case studies with known parameters simulating conditions known to be an issue in cyclostratigraphy (Sinnesael et al., 2019). Issues relating to cyclostratigraphy are: (1) Potential false negatives and positives in statistical hypothesis testing in power spectrum; (2) the completeness of the stratigraphic record (e.g. hiatuses); (3) uncertainties in the astronomical parameters in the deep-time geological past; (4) independent age control in cyclostratigraphy (Sinnesael et al., 2019). The issues are addressed in following ways: the issue of false negatives and positives are mitigated with the LOWSPEC analysis and the selection criteria used for the significant peaks (Meyers, 2012). The issues with the stratigraphic record's completeness are mitigated by sampling in sections without hiatuses and in deep marine mudstones, which tends to be more stratigraphically complete than coarser-grained siliciclastic successions from shallow marine environments (Weedon et al., 1999). The issue of uncertainty in the astronomical cycles is mitigated through the uncertainty ranges on the Milankovitch cycles (Table 1). Independent age control is available for core 7230/05-U-02 (Georgiev et al., 2017), but not for core 6307/07-U-03A. This means that the absolute time is uncertain for core 6307/07-U-03A. However, the start of the deposition of the Hekkingen Formation in the Late Oxfordian (157.7 ±1.3 Ma) is a reasonable time to correlate the section to. All major issues were addressed, so it is therefore reasonable to argue that the results are reliable, even though the uncertainties are hard to quantify. The TimeOpt optimal average sedimentation rates will be used in the astrochronological analysis, because of the likely orbital cycles detected in the significant peaks by the ratio method.

6.2. Influences on the Magnetic Signal and the Cyclicity

Mutterlose et al. (2003) and Langrock et al. (2003) investigated the palaeoenvironment of the Greenland-Norwegian Seaway during the Late Jurassic to Early Cretaceous. Mutterlose et al. (2003) state that the bedding patters in the seaway indicate orbital control on the climate causing changes in circulation, biological productivity, and degree of oxygenation in the water. Eccentricity, precession, and obliquity cycles are all present in the Greenland-Norwegian Seaway according to Mutterlose et al. (2003). All the Milankovitch cycles were identified in this work, supporting the statement from Mutterlose et al. (2003). Mutterlose et al. (2003) detected three sedimentary cycles. Type A cycles are caused by variation in the carbonate content and the bioturbation pattern, type B cycles are related to an alternation between black shale and siderite/dolomite concretions, and type C cycles are described as an alternation between black shales and silt laminae; in this period the depositional environment was characterised by clastic impulses controlled by astronomical forcing. Type A and B cycles may come from short term fluctuation in the sea level, with Type B cycles possibly reflect elevated surface productivity and TOC burial in sulphate reducing settings according to Mutterlose et al. (2003). Bugge et al. (2002) recorded a variation in the TOC content in the Hekkingen Formation in core 7230/05-U-02 between 7 and 23 wt%. The variation in TOC may reflect the Type A cycle Mutterlose et al. (2003) described. In the black shale section, Type B cycles of siderite concretions from iron-rich black shale facies shows evenly spaced beds in the cores related to the short eccentricity cycle (95 ka).

The magnetic susceptibility values between $4.0 - 12.0 \times 10^{-8}\ \mathrm{m^3 kg^{-1}}$ in core 6307/07-U-03A and $3.0 - 6.0 \times 10^{-8}\ \mathrm{m^3 kg^{-1}}$ in core 7230/05-U-02 are similar to the range of magnetic susceptibility values Boulila et al. (2010) described as characteristic for paramagnetic behaviour in clayey and marly sediments. This description corresponds well with the background magnetic susceptibility values in the laminated black shale facies.

The iron-rich black shale facies (Table 3) is present in both core 6307/07-U-03A and 7230/05-U-02. Most of the beds and laminae with the iron-rich black shale have a higher magnetic susceptibility than the main laminated black shale facies (Figure 8 and Figure 9). The correlation between iron-rich black shales and high magnetic susceptibility values is especially apparent in the Spekk Formation in core 6307/07-U-03A. The minerals that chiefly affect the magnetic measurements in the laminae and beds of iron-rich black shale are nodules and cement of siderite, shown by the high magnetic susceptibility values in siderite beds in core 6307/07-U-03A (Figure 10). Mørk et al. (2002) investigated the role of siderite in the magnetic susceptibility on Mesozoic sediments off Mid Norway in the Norwegian Sea, among them core 6307/07-U-03. They found relatively high susceptibility in the shaly Upper Jurassic sequences, and a positive correlation between high magnetic susceptibility and diagenetic siderite-cementation, particular in controlling the magnetic susceptibility in the black shale units. Mørk et al. (2002) could not find evidence for more magnetic minerals such as magnetite and pyrrhotite in the siderite grains of selected high susceptibility samples. The range of the magnetic

susceptibility values is from 123 to 998 $\times\ 10^{-6}$ SI in the siderite-rich beds in core 6307/07-U-03A, within the range of magnetic susceptibility values Mørk et al. (2002) measured in the siderite-rich samples. Pyrite is weakly paramagnetic, so the impact on magnetic susceptibility is small (Weedon et al., 2004), demonstrated by a lack of significant change in the magnetic susceptibility values in pyrite cemented beds in core 7230/05-U-02 (Figure 9).

The time series from the Spekk Formation with the high susceptibility siderite beds included has periods corresponding to the 95 ka short eccentricity cycle, and the 38 ka obliquity cycle (Table 4). The optimal sedimentation rate calculated by the TimeOpt method (Period A) and the sedimentation rate from Mutterlose et al. (2003) produces the 95 ka eccentricity cycle. The time series without the siderite beds has periods corresponding to the 38 ka obliquity cycle and ~20 ka precession cycles (Table 5). The short eccentricity cycle (95 ka) is only present in the time series with the siderite beds included, suggesting that the siderite beds caused the short eccentricity cycle (95 ka).

The sandy and silty shales at the top of core 7230/05-U-02 from ~36 m have an average magnetic susceptibility of $\sim 3.2 \times 10^{-8}\,\mathrm{m^3kg^{-1}}$ lower than the average magnetic susceptibility of $\sim 4.5 \times 10^{-8}\,\mathrm{m^3kg^{-1}}$ in the rest of the core (Figure 9). The source of the magnetic susceptibility is predominantly concentrated in the clay and silt fraction of the sediments according to Hounslow et al. (1995), and clay minerals are the primary control on the magnetic susceptibility. Therefore, the lower fraction of clay minerals in the upper part of the core may account for the lower magnetic susceptibility values. Using the optimal sedimentation rates calculated by the TimeOpt method, the significant frequencies in the whole section of the Hekkingen Formation have periods corresponding to the 95 ka eccentricity cycle, and ~20 ka precession cycles (Table 6). A significant change in the dominant frequencies occurs around 40 m in the core. The change coincides with a higher content of silt and fine sand, yielding a lower magnetic susceptibility in the upper section of the core from 40 m to 33.15 m. A power spectrogram in the upper interval from 40 m to 33.15 m identified a significant peak corresponding to the 38 ka obliquity cycle (Table 7), suggesting a change in the dominant astronomical period coinciding with a change in the depositional environment or variation in sedimentation rates.

6.3. Past Study of Milankovitch Cycles in the Black Shales of the Hekkingen Formation

Qvam (2018) performed cyclostratigraphic analysis on the black shales of the Hekkingen Formation and found similar cycles in different sections of core 7018/05-U-01 drilled in the Harstad Basin of the Barents Sea, and core 7430/10-U-01 North of the Nordkapp Basin in the Barents Sea. Core 7230/05-U-02 is located in the Nordkapp Basin of the Barents Sea, and the sedimentation rates used are similar, so it is reasonable to compare the cycles in core 7230/05-U-02 to the cycles identified by Qvam (2018). Qvam (2018) found cycles in durations between 34 ka and 35 ka in the core from the Harstad Basin, and 43.2 ka in the cores North of the Nordkapp

Basin. The cycles are comparable to the cycle of 40.3 ka in the present work in core 7230/05-U-02 (Table 7). Qvam (2018) also found cycles with a duration of 21.1 ka to 24.2 ka and 66.3 ka to 99.9 ka in the core North of the Nordkapp Basin, similar to the 19.3 ka and 95 ka cycles found in core 7230/05-U-02 from the Nordkapp Basin. The similarities in the identified cycles across the black shales in the Barents Sea indicate similar depositional environments across the Barents Sea in the Late Jurassic.

6.4. Astrochronology and Correlation

An astrochronology constructed by tuning the long eccentricity cycle (405 ka) for core 6307/07-U-03A and 7230/05-U-02 is shown in Figure 25. Four long eccentricity (405 ka) cycles are present in the section in both cores, with shorter eccentricity cycles of ~95 to ~124 ka superimposed on the long eccentricity cycles. The amplitude modulation of precession can be used for the correlation of cores at different locations where the black shales are deposited. The correlation assumes that the depositional environment in the Norwegian Sea and the Barents Sea responded in the same way to the astronomical cycles, generating long eccentricity cycles at the same time. Correlation is performed on the long eccentricity cycle, due to the high stability of the cycle with geological time (Laskar et al., 2004).

The total duration of the 19.8 m section in core 6307/07-U-03A is estimated to be 1.67 Ma. Dating for the base of the Spekk Formation is not available. However, the radiometrically dated age of the Hekkingen Formation base is ~157.7 ±1.3 Ma (Georgiev et al., 2017). The age of the base can be used as an absolute point in time for the duration of the 19.8 m section of the Spekk Formation, assuming the deposition of black shales of the Spekk Formation started at the same time as the deposition of the black shales of the Hekkingen Formation. The Spekk Formation was deposited from the Oxfordian age (161.2 Ma to 155.6 Ma), according to Dalland et al. (1988), so the assumption is reasonable. The radiometrically dated age of the base of the formation combined with the duration of the section determined the astrochronology results in an age from 157.70 ±1.3 Ma to 156.03 ±1.3 Ma, corresponding to a Late Oxfordian to Early Kimmeridgian age for the 19.8 m section of the Spekk Formation in core 6307/07-U-03A (Figure 25). The total duration of the 18.9 m section in core 7230/05-U-02 is estimated to be 1.68 Ma, nearly identical with the section from the Spekk Formation. The radiometrically dated age of the base of the formation combined with the duration of the section determined the astrochronology results in an age from 157.70 ±1.3 Ma to 156.02 ±1.3 Ma, corresponding to a Late Oxfordian to Early Kimmeridgian age for the 18.9 m section of the Hekkingen Formation in core 7230/05-U-02 (Figure 25).

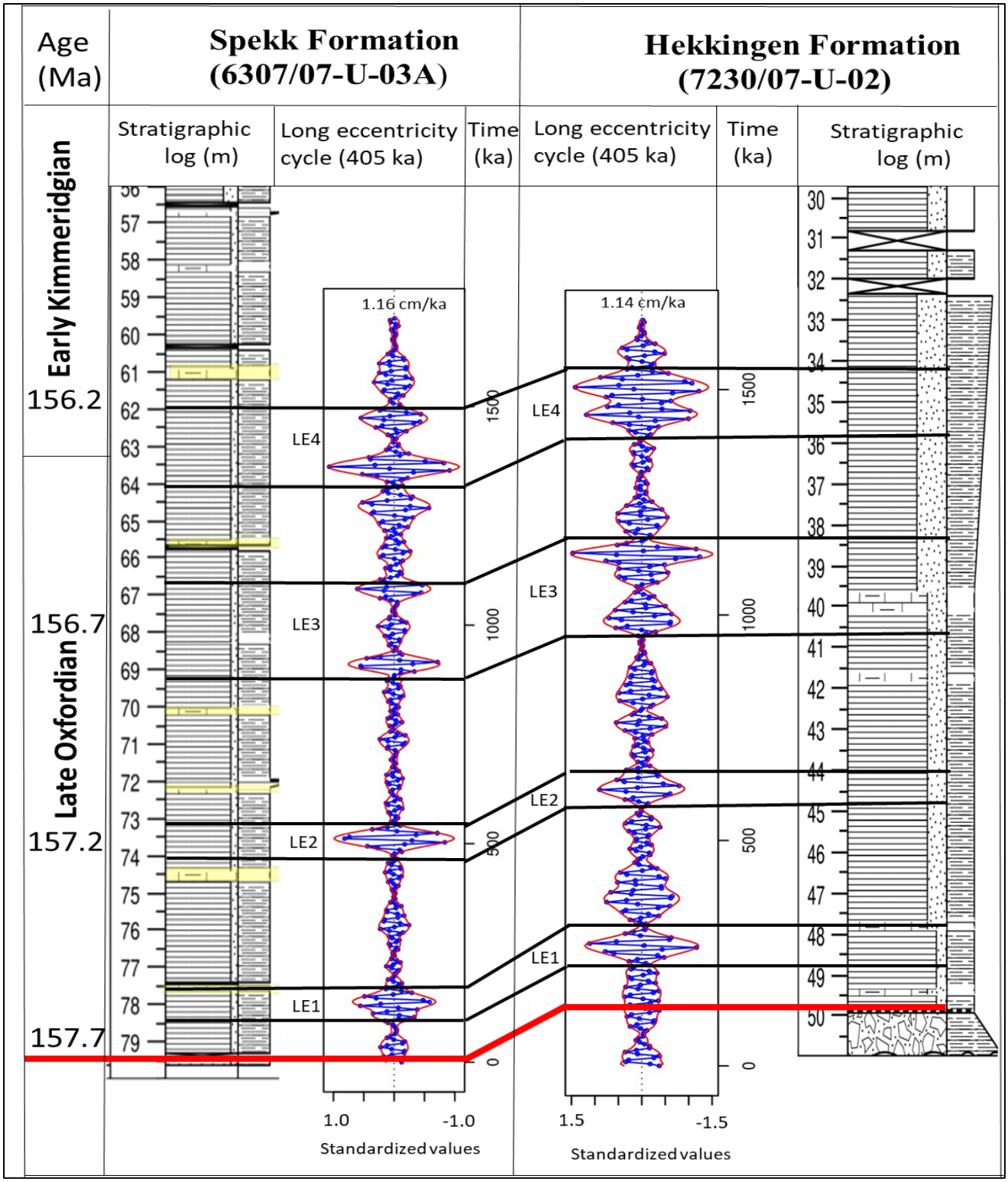

Figure 25. *Astrochronology calibrated with the tuned astronomical time series from the Milankovitch cycles. Correlation of the core from Spekk Formation (6307/07-U-03A), and the core from the Hekkingen Formation (7230/05-02) with the long eccentricity cycle (405 ka). The time series is made by comparing the band-passed precession signal (blue), and the data amplitude envelope (red) of the cores. An average sedimentation rate of 1.16 cm/ka for the Spekk Formation and an average sedimentation rate of 1.14 cm/ka for the Hekkingen Formation were used based on the optimization of sedimentation rates. LE: long eccentricity cycle (405 ka). The red line indicates the base of the Spekk and Hekkingen Formation radiometrically dated by Georgiev et al. (2017).*

7. Conclusion

From logging of cores containing Late Jurassic sediments in the Froan Basin of the Norwegian Sea (6307/07-U-03A), and the Nordkapp Basin of the Barents Sea (7230/05-U-02), six facies were identified. Laminated black shale is the dominant facies in the Late Jurassic deposits in the cores. Facies consisting of iron-rich black shales containing diagenetic siderite and pyrite cemented beds is also present throughout the logged section of both cores. A general upward coarsening sequence is present in the cores. Black shale is present in the lower parts of the logged sections, and muddy sandstone to sandstone facies in the upper part of core 6307/07-U-03A, and sandy and silty shales in the upper part of core 7230/05-U-02.

Magnetic susceptibility was used to determine the signal used in the cyclostratigraphic analysis. The highest average values are recorded in the siderite-rich shale facies, and the lowest average susceptibility values are recorded in the muddy sandstone and sandstone facies in core 6307/07-U-03A, and shales with a higher content of sand and silt in core 7230/05-U-02.

Measurements of rock magnetic susceptibility in black shales from the Spekk and Hekkingen Formation record cycles in the Milankovitch bands. Cycle lengths of significant periods of 5.5 m, 1.2 m, 0.32 m, and 0.15 m corresponding to the long eccentricity cycle (405 ka), short eccentricity cycle (95 ka), obliquity cycle (38 ka), and precession cycles (~18.2 ka) were identified in the black shales from the Froan Basin (6307/07-U-03A). Cycle lengths of significant periods of 1.1 m, 0.45 m, and 0.2 m corresponding to the short eccentricity cycle (95 ka), the obliquity cycle (38 ka), and the precession cycles (~18.2 ka) were identified in the black shales from the Nordkapp Basin (7230/05-U-02).

Variation in the dominant frequency throughout the cores suggests a fluctuation in the sedimentation rate. The average sedimentation rate used to calculate the duration of the significant peaks was estimated based on the simultaneous optimization of amplitude modulation of the precessional band and the ratio of the expected astronomical period. The sedimentation rates generate periods within a time frame equivalent to the Milankovitch cycles. The sedimentation rates were used to construct an astrochronology based on the time series tuned to the long eccentricity cycle (405 ka) and correlated to radiometric dates. The long eccentricity cycles (405 ka) in the time series were utilized in correlation of the two cores. In core 6307/07-U-03A the estimated average sedimentation rate is 1.19 cm/ka with a variation between 1.15 cm/ka to 1.64 cm/ka, leading to a total duration in the 19.8 m section of 1.67 Ma. In core 7230/05-U-02 the average sedimentation rate is 1.14 cm/ka with a variation between 0.84 cm/ka to 1.81 cm/ka cm/ka, leading to a total duration of the 18.9 m section of 1.68 Ma. The tuned time series reveal four long eccentricity cycles (405 ka) in the cores, with shorter cycles corresponding to the short eccentricity cycles (95 ka and 124 ka) superimposed on the long eccentricity cycle.

8. References

Berger, A. (1976) Obliquity and precession for the last 5 000 000 years. *Astronomy and Astrophysics*, **51,** 127-135.

Berger, A. (1978) Long-term variations of daily insolation and Quaternary climatic changes. *Journal of the Atmospheric Sciences*, **35,** 2362-2367.

Berger, A. (1988) Milankovitch theory and climate. *Reviews of Geophysics*, **26,** 624-657.

Berger, A. (2012) A brief history of the astronomical theories of paleoclimates. In: *Climate Change* (Ed M.F. Berger A, Sijacki D), pp. 107-129. Springer Vienna.

Blystad, P. (1995) *Structural elements of the Norwegian continental shelf, Part II : The Norwegian Sea region*. NPD-bulletin 8, Stavanger, Norway.

Boggs Jr, S. and Boggs, S. (2009) *Petrology of sedimentary rocks*. Cambridge University Press, Cambridge, UK, 600 pp.

Boulila, S., Galbrun, B., Hinnov, L.A., Collin, P.Y., Ogg, J.G., Fortwengler, D. and Marchand, D. (2010) Milankovitch and sub-Milankovitch forcing of the Oxfordian (Late Jurassic) Terres Noires Formation (SE France) and global implications. *Basin Research*, **22,** 717-732.

Brekke, H. and Riis, F. (1987) Tectonics and basin evolution of the Norwegian shelf between 62 N and 72 N. *Norsk Geologisk Tidsskrift*, **67,** 295-322.

Bugge, T., Elvebakk, G., Fanavoll, S., Mangerud, G., Smelror, M., Weiss, H.M., Gjelberg, J., Kristensen, S.E. and Nilsen, K. (2002) Shallow stratigraphic drilling applied in hydrocarbon exploration of the Nordkapp Basin, Barents Sea. *Marine and Petroleum Geology*, **19,** 13-37.

Bugge, T., Mangerud, G., Elvebakk, G., Mørk, A., Nilsson, I., Fanavoll, S. and Vigran, J.O. (1995) The Upper Palaeozoic succession on the Finnmark Platform, Barents Sea. *Norsk Geologisk Tidsskrift*, **75,** 3-30.

Collins, D. and Bras, R. (2008) Climatic control of sediment yield in dry lands following climate and land cover change. *Water Resources Research*, **44**.

Dalland, A., Worsley, D. and Ofstad, K. (1988) A lithostratigraphic scheme for the Mesozoic and Cenozoic succession offshore mid-and northern Norway, NPD-Bulletin No. 4. *Stavanger, Norway*.

Faleide, J.I., Gudlaugsson, S.T. and Jacquart, G. (1984) Evolution of the western Barents Sea. *Marine and Petroleum Geology*, **1,** 123-150.

Gabrielsen, R.H., Foerseth, R., Hamar, G. and Rønnevik, H. (1984) Nomenclature of the main structural features on the Norwegian Continental Shelf north of the 62nd parallel. In: *Petroleum Geology of the North European Margin* (Ed A.M. Spencer), pp. 41-60. Springer, Dordrecht.

Georgiev, S.V., Stein, H.J., Hannah, J.L., Xu, G., Bingen, B. and Weiss, H.M. (2017) Timing, duration, and causes for Late Jurassic–Early Cretaceous anoxia in the Barents Sea. *Earth and Planetary Science Letters*, **461,** 151-162.

Hamar, G., Fjaeran, T. and Hesjedal, A. (1983) Jurassic stratigraphy and tectonics of the south-southeastern Norwegian offshore. In: *Petroleum geology of the southeastern North Sea and the adjacent onshore areas* (Eds T.J.A. Reijers and J.P.H. Kaasschieter), pp. 103-114. Springer, Dordrecht.

Hays, J.D., Imbrie, J. and Shackleton, N.J. (1976) Variations in the Earth's orbit: pacemaker of the ice ages. *Science*, **194,** 1121-1132.

Hinnov, L.A. (2013) Cyclostratigraphy and its revolutionizing applications in the earth and planetary sciences. *Geological Society of America*, **125,** 1703-1734.

Hounslow, M.W., Maher, B.A. and Thistlewood, L. (1995) Magnetic mineralogy of sandstones from the Lunde Formation (late Triassic), northern North Sea, UK: origin of the palaeomagnetic signal. In: *Palaeomagnetic Applications in Hydrocarbon Exploration and Production* (Eds P. TURNER and A. TURNER), pp. 119-147, Geological Society Special Publication No. 98.

Huang, C., Hesselbo, S.P. and Hinnov, L. (2010) Astrochronology of the late Jurassic Kimmeridge Clay (Dorset, England) and implications for Earth system processes. *Earth and Planetary Science Letters*, **289,** 242-255.

Kodama, K.P. (2019) Rock Magnetic Cyclostratigraphy of the Carboniferous Mauch Chunk Formation, Pottsville, PA, United States. *Frontiers in Earth Science*, **7**.

Kodama, K.P. and Hinnov, L.A. (2014) *Rock magnetic cyclostratigraphy*. Wiley-Blackwell, Oxford, UK, 176 pp.

Langbein, W.B. and Schumm, S.A. (1958) Yield of sediment in relation to mean annual precipitation. *Eos, Transactions American Geophysical Union*, **39,** 1076-1084.

Langrock, U., Stein, R., Lipinski, M. and Brumsack, H.J. (2003) Late Jurassic to Early Cretaceous black shale formation and paleoenvironment in high northern latitudes: examples from the Norwegian-Greenland Seaway. *Paleoceanography*, **18**.

Laskar, J., Robutel, P., Joutel, F., Gastineau, M., Correia, A. and Levrard, B. (2004) A long-term numerical solution for the insolation quantities of the Earth. *Astronomy & Astrophysics*, **428,** 261-285.

Loseth, H. and Tveten, E. (1996) Post-Caledonian structural evolution of the Lofoten and Vesteralen offshore and onshore areas. *Norsk Geologisk Tidsskrift*, **76,** 215-229.

Meyers, S. (2014) Astrochron: An R package for astrochronology, http://cran.rproject.org/package=astrochron.

Meyers, S.R. (2012) Seeing red in cyclic stratigraphy: Spectral noise estimation for astrochronology. *Paleoceanography*, **27**.

Meyers, S.R. (2015) The evaluation of eccentricity-related amplitude modulation and bundling in paleoclimate data: An inverse approach for astrochronologic testing and time scale optimization. *Paleoceanography*, **30,** 1625-1640.

Meyers, S.R., Sageman, B.B. and Hinnov, L.A. (2001) Integrated quantitative stratigraphy of the Cenomanian-Turonian Bridge Creek Limestone Member using evolutive harmonic analysis and stratigraphic modeling. *Journal of Sedimentary Research*, **71,** 628-644.

Mutterlose, J., Brumsack, H., Flögel, S., Hay, W., Klein, C., Langrock, U., Lipinski, M., Ricken, W., Söding, E. and Stein, R. (2003) The Greenland-Norwegian Seaway: A key area for understanding Late Jurassic to Early Cretaceous paleoenvironments. *Paleoceanography*, **18**.

Mørk, M. and Johnsen, S. (2005) Jurassic sandstone provenance and basement erosion in the Møre margin–Froan Basin area. *Norges geologiske undersøkelse Bulletin 443*, 5-18.

Mørk, M.B.E., McEnroe, S.A. and Olesen, O. (2002) Magnetic susceptibility of Mesozoic and Cenozoic sediments off Mid Norway and the role of siderite: implications for interpretation of high-resolution aeromagnetic anomalies. *Marine and Petroleum Geology*, **19,** 1115-1126.

Mørk, M.B.E., Vigran, J.O., Smelror, M., Fjerdingstad, V. and Bøe, R. (2003) Mesozoic mudstone compositions and the role of kaolinite weathering-a view from shallow cores in the Norwegian Sea (Møre to Troms). *Norwegian Journal of Geology/Norsk Geologisk Forening*, **83,** 61-78.

NPD (2019) NPD FactMaps 2.0 edn, https://factmaps.npd.no/factmaps/3_0/ (20.11.19).

Nøttvedt, A., Cecchi, M., Gjelberg, J.G., Kristensen, S.E., Lønøy, A., Rasmussen, A., Rasmussen, E., Skott, P.H. and van Veen, P.M. (1993) Svalbard-Barents Sea correlation: a short review. In: *Arctic Geology and Petroleum Potential* (Eds T.O. Vorren, E. Bergsager, O.A. Dahl-Stamnes, E. Holter, B. Johansen, E. Lie and T.B. Lund), pp. 363-375. Norwegian Petroleum Society Special Publications 2, Elsevier, Amsterdam.

Pederson, J., Pazzaglia, F. and Smith, G. (2000) Ancient hillslope deposits: Missing links in the study of climate controls on sedimentation. *Geology*, **28,** 27-30.

Potter, P.E., Maynard, J.B. and Depetris, P.J. (2005) *Mud and mudstones: Introduction and overview*. Springer, Berlin, Heidelberg, New York, 297 pp.

Qvam, E.S. (2018) *Relationship between environmental conditions and magnetic properties of Norwegian black shales*, NTNU, Unpublished MSc thesis, 111 pp.

R-CoreTeam (2019) R: A language and environment for statistical computing. Vienna: R Foundation for Statistical Computing, http://www.R-project.org/.

Rise, L. and Sættem, J. (1994) Shallow stratigraphic wireline coring in bedrock offshore Norway. *Scientific Drilling*, **4,** 243-257.

Sinnesael, M., De Vleeschouwer, D., Zeeden, C., Batenburg, S.J., Da Silva, A.-C., de Winter, N.J., Dinarès-Turell, J., Drury, A.J., Gambacorta, G. and Hilgen, F.J. (2019) The Cyclostratigraphy Intercomparison Project (CIP): consistency, merits and pitfalls. *Earth-Science Reviews*, **199**.

Smelror, M., Mørk, A., Mørk, M.B.E., Weiss, H.M. and Løseth, H. (2001) Middle Jurassic-Lower Cretaceous transgressive-regressive sequences and facies distribution off northern Nordland and Troms, Norway. In: *Sedimentary environments offshore Norway-Palaeozoic to Recent* (Eds O. Martinsen and T. Dreyer), **10**, pp. 211-232. Elsevier, Amsterdam, Norwegian Petroleum Society (NPF) Special Publication 10.

Swientek, O. (2002) *The Greenland Norwegian Seaway: climatic and cyclic evolution of Late Jurassic-Early Cretaceous sediments*, Universität zu Köln, 119 pp.

Thomson, D.J. (1982) Spectrum estimation and harmonic analysis. *Proceedings of the IEEE*, **70,** 1055-1096.

Waltham, D. (2015) Milankovitch period uncertainties and their impact on cyclostratigraphy. *Journal of Sedimentary Research*, **85,** 990-998.

Weedon, G.P., Coe, A.L. and Gallois, R.W. (2004) Cyclostratigraphy, orbital tuning and inferred productivity for the type Kimmeridge Clay (Late Jurassic), Southern England. *Journal of the Geological Society*, **161,** 655-666.

Weedon, G.P., Jenkyns, H.C., Coe, A.L. and Hesselbo, S.P. (1999) Astronomical calibration of the Jurassic time-scale from cyclostratigraphy in British mudrock formations. *Philosophical Transactions of the Royal Society of London. Series A: Mathematical, Physical and Engineering Sciences*, **357,** 1787-1813.

Wierzbowski, A. and Smelror, M. (1993) Ammonite succession in the Kimmeridgian of southwestern Barents Sea, and the Amoeboceras zonation of the Boreal Kimmeridgian. *Acta Geologica Polonica*, **43,** 229-250.

Worsley, D. (2008) The post-Caledonian development of Svalbard and the western Barents Sea. *Polar Research*, **27,** 298-317.

Xu, Y., Haykin, S. and Racine, R.J. (1999) Multiple window time-frequency distribution and coherence of EEG using Slepian sequences and Hermite functions. *IEEE Transactions on Biomedical Engineering*, **46,** 861-866.

Zervas, D., Nichols, G.J., Hall, R., Smyth, H.R., Luthje, C. and Murtagh, F. (2009) SedLog: A shareware program for drawing graphic logs and log data manipulation. *Computers & Geosciences*, **35,** 2151-2159.

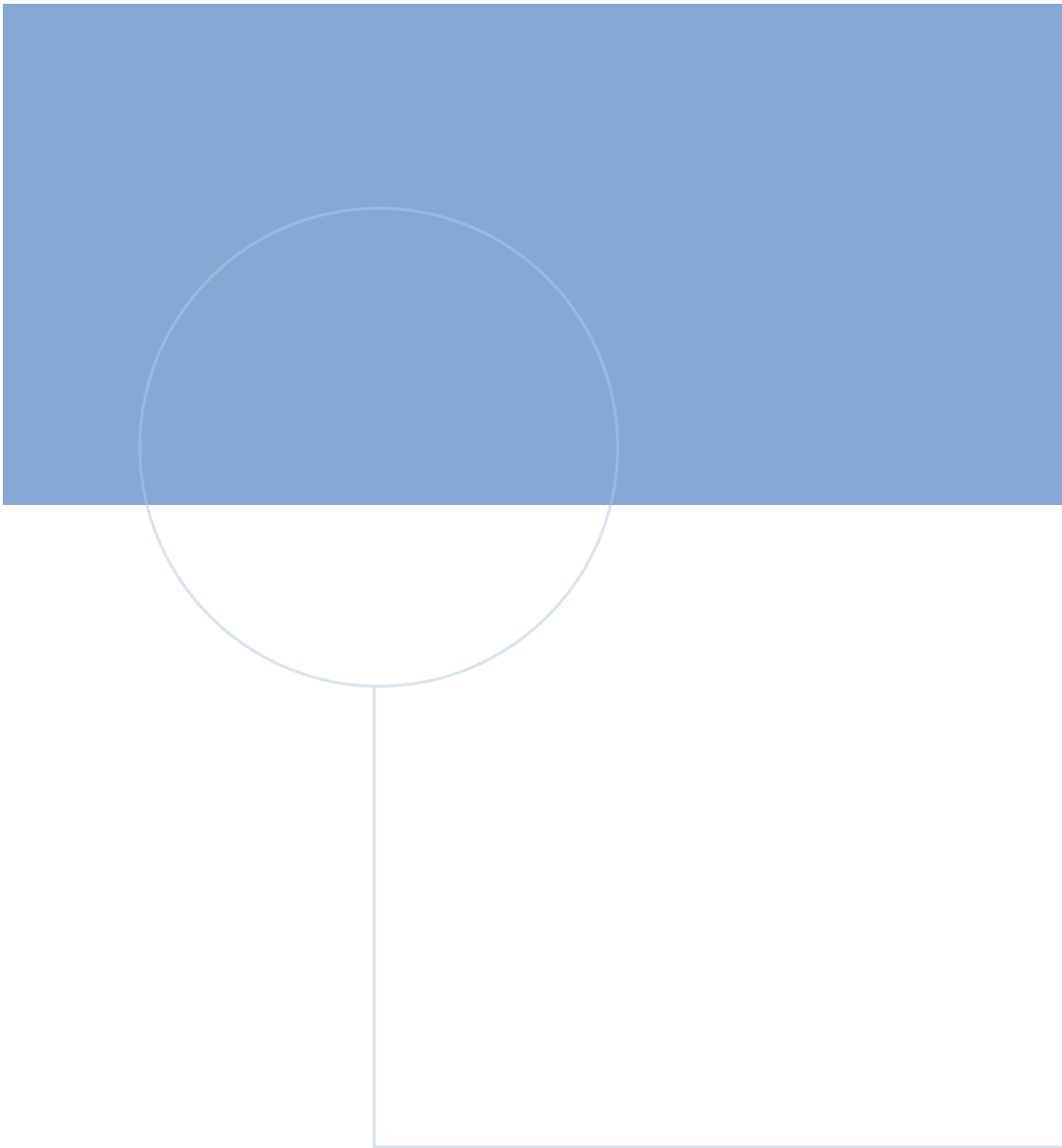

NTNU

Kunnskap for en bedre verden